ORIGINAL ARTICLE

Journal of Neurochemistry | JNC | The Official Journal of the International Society for Neurochemistry | WILEY

Transcriptomic, peptidomic, and mass spectrometry imaging analysis of the brain in the ant *Cataglyphis nodus*

Jens Habenstein[1] [iD] | Franziska Schmitt[1] | Sander Liessem[2] [iD] | Alice Ly[3] | Dennis Trede[4] | Christian Wegener[5] [iD] | Reinhard Predel[2] [iD] | Wolfgang Rössler[1] [iD] | Susanne Neupert[2,6] [iD]

[1]Behavioral Physiology and Sociobiology (Zoology II), University of Würzburg, Würzburg, Germany

[2]Department of Biology, Institute for Zoology, University of Cologne, Cologne, Germany

[3]Bruker Daltonik GmbH, Bremen, Germany

[4]SCiLS, Zweigniederlassung Bremen der Bruker Daltonik GmbH, Bremen, Germany

[5]Theodor-Boveri-Institute, Neurobiology and Genetics, Würzburg Insect Research, University of Würzburg, Würzburg, Germany

[6]Department of Biology, University of Kassel, Kassel, Germany

Correspondence
Susanne Neupert, Department for Biology, Animal Physiology, University of Kassel, Heinrich-Plett-Strasse 40, 34132 Kassel, Germany
Email: mail@susanne-neupert.de

Jens Habenstein
Biocenter, Behavioral Physiology and Sociobiology (Zoology II), University of Würzburg, Am Hubland, 97,074 Würzburg, Germany.
Email: jens.habenstein@uni-wuerzburg.de

Abstract

Behavioral flexibility is an important cornerstone for the ecological success of animals. Social *Cataglyphis nodus* ants with their age-related polyethism characterized by age-related behavioral phenotypes represent a prime example for behavioral flexibility. We propose neuropeptides as powerful candidates for the flexible modulation of age-related behavioral transitions in individual ants. As the neuropeptidome of *C. nodus* was unknown, we collected a comprehensive peptidomic data set obtained by transcriptome analysis of the ants' central nervous system combined with brain extract analysis by Q-Exactive Orbitrap mass spectrometry (MS) and direct tissue profiling of different regions of the brain by matrix-assisted laser desorption/ionization time-of-flight (MALDI-TOF) MS. In total, we identified 71 peptides with likely bioactive function, encoded on 49 neuropeptide-, neuropeptide-like, and protein hormone prepropeptide genes, including a novel neuropeptide-like gene (*fliktin*). We next characterized the spatial distribution of a subset of peptides encoded on 16 precursor proteins with high resolution by MALDI MS imaging (MALDI MSI) on 14 μm brain sections. The accuracy of our MSI data were confirmed by matching the immunostaining patterns for tachykinins with MSI ion images from consecutive brain sections. Our data provide a solid framework for future research into spatially resolved qualitative

and quantitative peptidomic changes associated with stage-specific behavioral transitions and the functional role of neuropeptides in *Cataglyphis* ants.

1 | INTRODUCTION

Insect societies operate as cohesive units, even though individual colony members may express very different behavioral phenotypes contributing to diverse tasks (Hölldobler & Wilson, 1990). To ensure a dynamic and successful interplay of the insects within a colony, task allocation needs to be orchestrated in response to various internal and external cues (for reviews see: Beshers & Fewell, 2001; Robinson, 1992). External cues such as the availability of food, stimuli that signal the need for a specific task, or the demographic composition of the colony, directly affect the task performance and can induce short-term task switches (Gordon, 1989, reviewed by: Robinson, 1992, Yang, 2006). In addition, individuals follow innate behavioral patterns. These are often related to age. For example, young individuals fulfill tasks inside the nest, whereas older individuals primarily perform completely different and riskier tasks outside the nest (for reviews see: Hölldobler & Wilson, 1990; Oster & Wilson, 1978).

Age-related behavioral plasticity in social insects was shown to be associated with changes in diverse neuromodulators and hormones (reviewed by: Hamilton et al., 2016). Variations in biogenic amine levels (Wagener-Hulme et al., 1999, Seid & Traniello, 2005, reviewed by: Kamhi & Traniello, 2013), juvenile hormone titers (Bloch et al., 2002; Ddolezal et al., 2012; Robinson, 1987), and vitellogenin levels (Amdam & Omholt, 2003; Gospocic et al., 2017; Kohlmeier et al., 2018) at the transition from interior worker to forager are prominent examples. However, the causal contribution of these messenger molecules to changes in specific behaviors were discussed controversially (Huang & Robinson, 1995, Sullivan et al., 2000, Scholl et al., 2014, reviewed by: Hamilton et al., 2016). Recent studies, therefore, started to focus on neuropeptides as potential regulators of specific behavioral patterns and their transitions in social Hymenoptera (*e.g.* Takeuchi et al., 2003, Brockmann et al., 2009, Pratavieira et al., 2014, 2018; Han et al., 2015, Schmitt et al., 2017, Gospocic et al., 2017).

Neuropeptides represent a very large and diverse group of intercellular messenger molecules. They are processed from larger precursor proteins (preproprotein) by a set of dedicated enzymes that cleave the proprotein at specific sites (Fricker, 2012; Pauls et al., 2014), and typically act as neurohormones or neuromodulators (for reviews see: Fricker, 2012; Nässel & Zandawala, 2019; Schoofs et al., 2017). Neuropeptides orchestrate diverse behaviors as well as physiological and developmental processes (for reviews see: Fricker, 2012; Kastin, 2013; Nässel & Zandawala, 2019).

In insects, neuropeptides modulate for instance general locomotor activity (Kahsai, Martin et al., 2010), feeding (Ko et al., 2015, Chen et al., 2016, reviewed by: Schoofs et al., 2017), or olfactory memory (Knapek et al., 2013; Urlacher et al., 2016; Winther et al., 2006). Neuropeptides such as corazonin (Crz), tachykinin-related peptides (TK), or short neuropeptide *F* (sNPF) show different expression levels (protein/RNA) related to age, tasks or internal and behavioral stages in honey bees (Gospocic et al., 2017; Pratavieira et al., 2018; Takeuchi et al., 2003), wasps, and ants (Gospocic et al., 2017). In the same line, the distribution of allatostatin-A (Ast-A) and TK exhibit age-related changes within multisensory integration centers in the brain of the honey bee (Pratavieira et al., 2014) and *Cataglyphis* ants (Schmitt et al., 2017). These studies are highly suggestive for a key role of neuropeptides in the flexible regulation of distinct behavioral phenotypes in social insects, particularly at the transition from nursing behavior inside the dark nest to the performance of outdoor foraging. The marked behavioral transitions in thermophilic ants of the genus *Cataglyphis* Foerster, 1,850 (Hymenoptera, Formicidae) provide an excellent experimental model to investigate mechanisms of neuronal plasticity underlying age-related behavioral plasticity (Rössler, 2019). After several interior stages with tasks inside the darkness of the nest which last about four weeks, the ants leave the nest for the first time to perform learning walks close to the nest entrance under bright sunlight for 2–3 days (Fleischmann et al., 2017, 2018). Immediately after completing their learning walks, the ants start to search for food by performing primarily visually guided foraging trips that may span over remarkable distances of up to several hundred meters (reviewed in Ronacher, 2008; Rössler, 2019; Wehner, 2009).

To start to investigate the molecular mechanisms underlying such behavioral flexibility, genomics and transcriptomic data from various ant species are available (e.g. Warner et al., 2019; Wurm et al., 2011). Furthermore, neuropeptidergic data sets from the carpenter ant *Camponotus floridanus* (Schmitt et al., 2015) and the closely related desert ant *Cataclyphis fortis* (Schmitt et al., 2017) exist, however, comparable genetic and biochemical data in the important experimental model ant *C. nodus* are missing so far. Recently, a three-dimensional brain atlas was published for this ant by mapping 33 synapse-rich neuropil regions and 30 interconnecting fiber tracts, among them are six parallel visual pathways (Habenstein et al., 2020; neuronal cell bodies are mostly on the cortex of the brain and were excluded). This first comprehensive neuroanatomical analysis of an ant brain revealed a highly complex compartmentalization of neuronal processes in a small brain. Until now, however, nothing is known

about the distribution of signaling molecules such as neuropeptides within the *C. nodus* brain. As a prerequisite to better understand the functional role of neuropeptides within the neurocircuits in the nervous system of this social insect model, we here started by analyzing the transcriptome of the *C. nodus* brain for neuropeptide sequences. We found 49 identified protein sequences from 31 genes encoding neuropeptides and neuropeptide-like substances. Next, we analyzed brain extracts of *C. nodus* by Q-Exactive Orbitrap MS and individual neuronal tissue samples by direct tissue profiling using MALDI-TOF MS to determine the actual set of processed neuroactive compounds including post-translational modifications (PTM). The most common PTMs in insects are the C-terminal amidation of the hydroxyl group of glycine, cyclization of the N-terminal glutamine and aspartate to pyroglutamic acid, formation of disulfide bridges formed between thiol groups in two cysteine residues and sulfation. The combination of MS methods had previously been successfully used by us to characterize the neuropeptidome of other insects, including ants (e.g. Liessem et al., 2018; Predel et al., 2018; Schmitt et al., 2015). Altogether, we identified 71 potential bioactive neuropeptides via mass matches in the brain of *C. nodus* whereas 56 peptides are confirmed by fragmentation experiments. Then, we localized subsets of the identified neuropeptides to specific brain compartments and neuropils in the brain by mass spectrometric imaging (MALDI-MSI).

In insects, MSI has been used for the first time for neuropeptide imaging from neuronal tissue samples of the cricket *Acheta domesticus* by a MALDI- ion trap (Verhaert et al., 2007). Previously, Pratavieira et al., (2014, 2018) used MALDI-TOF MSI to analyze developmental and state-dependent changes in the neuropeptide composition and distribution in the honey bee brain, yet these studies, although being successful, were restricted to a limited set of detected neuropeptides. Here, based on previously published protocols for neuropeptidergic MSI analysis of invertebrate tissue samples (e.g. Chen & Li, 2010; Ly et al., 2019; Pratavieira et al., 2014), we optimized and further developed sample preparation steps for MALDI-MSI of ant brains, and evaluated their accuracy comparing TK immunostaining and MALDI-MSI ion signal patterns on consecutive brain sections. Overall, we were able to obtain molecular images for peptides encoded on 16 genes.

The results of our comprehensive peptidomic study together with the MALDI-MSI procedure optimized for ant brains now open the possibility to correlate brain-wide peptidomic changes and test their function on modulation of dynamic behavioral phenotypes in manipulation experiments, in particular behaviors associated with polyethism in social insects like *C. nodus* ants.

2 | EXPERIMENTAL PROCEDURES

2.1 | Animals

C. nodus colonies were collected at Schinias National Park, Greece (38°15' N, 24°03' E) and transported to the Biocenter of the University of Würzburg. In Würzburg, the ants were kept in a climate chamber under 12:12 hr day/night conditions at 28°C and 20%–30% relative humidity. The animals had infinite access to water and were fed with dead cockroaches and honey diluted in water (1:2). For all studies, *Cataglyphis* workers were taken from queenless colonies. Age and previous experiences of individuals were unknown. Since all animals were picked arbitrarily, no randomization as well as no blinding was performed to allocate individual subjects in the study. In all experiments, adult ant brains were used without a specific sample size calculation. A number of at least four animals were tested in each experimental approach. This study was carried out in accordance with the Greek and German laws. Institutional ethics approval was not required for this study. The study was not pre-registered.

2.2 | Classification of analytes

In this study, we used the term neuropeptide for shorter peptide molecules of a length up to 45 aa produced by neuronal and endocrine cells and from larger preproproteins that contain a signal peptide and canonical prohormone convertase processing sites, and which are known in insects to execute functions as neuromodulator or hormone via G-protein-coupled receptor (GCPR)-signaling. Neuropeptide-like peptides are here defined as peptides which fulfilled most of the above criteria but for which the functions or receptors are unknown. Protein hormones are peptides larger than 45 aa which are produced by neuronal and endocrine cells from larger preproproteins that contain at least a signal peptide, and which are known in insects to be secreted into the haemolymph to regulate processes in distant target organs. Precursor peptides (PP) are biologically inactive shorter peptide sequences produced during preprotein processing which cannot be turned into an active form by posttranslational modification.

2.3 | Transcriptome analysis

- *RNA extraction*: Whole brains of *C. nodus* workers ($n = 12$) were preserved in TRIzol (Life Technologies Inc.) at 4°C according to the manufacturer´s recommendation. RNA analysis was implemented in Agilent 2,100 Bioanalyzer.
- *Library construction and transcriptome sequencing*: Libraries were sequenced using the Illumina Truseq RNA Sample Preparation Kit (Illumina) and sequencing was done using an Illumina TruSeq PE Cluster Kit v3 and an Illumina TruSeq 31 SBS Kit v3—HS on an Illumina HiSeq 4,000 sequencer with a paired-end by the Gene Expression Affymetrix facility at the CMMC at the University of Cologne (Germany). The library was sequenced for 100 bp paired-ends, which were stored as FASTQ files.
- De novo *assembly*: Raw data were initially filtered by removing adapters, reads with more than 5% of unknown bases and reads with low quality sequences (reads having more than 20% bases with quality value lower or equal to 10). Subsequently transcripts were de novo assembled using Trinity (v2.2.0) (Grabherr

et al., 2011; Haas et al., 2013) and Bridger (v2014-12-01) (Chang et al., 2015) with default options. De-novo assembly quality was assessed using TransRate (v1.0.3, Smith-Unna et al., 2016). The resulting RAW reads were filtered, by removing adapter sequences, contamination and low-quality reads using Trimmomatic 0.38 (Bolger et al., 2014) and submitted to NCBI (Sequence Read Archives (SRA): SRR10955559, BioProject: PRJNA602618, BioSample: SAMN13899910, Transcriptome Shotgun Assembly (TSA): pending for release. The quality of the assembly was subsequently assessed with TransRate: 106,977,131 bases and 76,048 contigs were included in the assembly. The N50 length, that is the largest contigs size at which 50% of bases are contained in contigs of at least this length, is 2,952.

- *Compiling of Precursor Sequences*: The tBLASTn algorithm from the BLAST + suite command-line tool (v2.4.0.) (Camacho et al., 2009) was used to conduct database searches for *C. nodus* neuropeptide precursor sequences. As reference queries, selected sequences of known insect neuropeptide precursors from different non-pterygote hexapods (Derst et al., 2016) and pterygote insects such as the honey bee *Apis mellifera* (Hummon et al., 2006), the yellow fever mosquito *Aedes agyptii* (Predel et al., 2010), the stick insect *Carausius morosus* (Liessem et al., 2018) and the two closely related ant species *Camponotus floridanus* (Schmitt et al., 2015) and *Cataglyphis fortis* (Schmitt et al., 2017) were used. Identified sequences were translated into proteins using ExPASy translate tool (http://web.expasy.org/translate/, Swiss Institute of Bioinformatics, Switzerland) (Gasteiger et al., 2003). Signal peptides (SP) were predicted using the SignalP 4.1 server (www.cbs.dtu.dk/services/SignalP/. Technical University of Denmark, Denmark). If no SP could be predicted or no stop codon was present, precursors were considered as incomplete. Cleavage sites, potential neuropeptides, and precursor peptides (PPs) were calculated by the NeuroPred server (http://stagbeetle.animal.uiuc.edu/cgi-bin/neuropred.py) and were manually assigned based on Veenstra (2000).

2.4 | Tissue preparation for mass spectrometry

Ants were anesthetized on ice and decapitated. Head capsules were opened and covered with ice-cold physiological insect saline (128 mM NaCl, 2.7 mM KCl, 2 mM $CaCl_2$, 1.2 mM $NaHCO_3$, pH 7.25).

- *Direct tissue profiling (n = 15)*: Brains with attached *corpora cardiaca* and *corpora allata* (retrocerebral complex) and gnathal ganglion (GNG) were removed and transferred into a drop of fresh saline. *Corpora cardiaca* and *corpora allata*, small parts of different brain areas and GNG were separately dissected and transferred using a glass capillary fitted to a tube with a mouth piece into a drop of water placed on a sample plate for MALDI-TOF MS analysis as described in Schachtner et al., (2010). Immediately after transfer, water was removed around the sample and the tissue was allowed to dry before matrix application. Only tissue samples that were not contaminated by other tissues such as fat were chosen for MS profiling.

- *Tissue extraction (in total n = 95)*: We made eight different sample sets, consisting of 2 × 20, 1 × 15, 3 × 10, and 2 × 5 brains/ GNGs. Each sample set was collected in 30 µl extraction solution containing 50% methanol, 49% H_2O, and 1% formic acid (FA) on ice. Tissue samples were homogenized using an ultrasonic bath (Transonic 660/H; Elma Schmidbauer GmbH) for 5 min on ice and then treated using an ultrasonic-finger (BandelinSono HD 200; Bandelin Electronic GmbH) three times for 5 s. Afterwards, the samples were centrifuged for 15 min at 13,000 rpm at 4°C. The supernatants were separated and then evaporated in a vacuum concentrator to remove methanol. Extracts were stored at −20°C until use.

- *MALDI-MSI (for protocol optimization: n = around 500 brain sections from around 100 brains; for final experiments: n = 12 brain sections [3 sections from 4 brains])*: Heads were fixed in wax-coated dishes and the head capsule was opened. To minimize peptide-release during the preparation, we rinsed the brains with ice-cold artificial ant saline solution (127 mM NaCl, 7 mM KCl, 1.5 mM CaCl2, 0.8 mM Na2HPO4, 0.4 mM KH2PO4, 4.8 mM TES, 3.2 mM trehalose, pH 7.0) and analyzed only brains for which the isolation procedure did not exceed 10 min. The brain was removed, rinsed in distilled water for a few seconds and embedded in gelatin (Dr. Oetker Gelatine Gold extra, Germany). For neuropeptide imaging experiments, gelatin is the embedding substrate of choice because it does not produce interfering signals in the neuropeptide mass range (m/z 600–4,000), unlike polymer-containing embedding media (Chen et al., 2009; Chen & Li, 2010; Khatib-Shahidi et al., 2006). Confirming Chen & Li, 2010, 100 mg/ml gelatin in water resulted in highly reproducible consecutive brain sections with high-quality mass spectra containing neuropeptide signals. For that, 100 mg/ml gelatin was completely dissolved in distilled water at 50°C and poured into 5 × 5 × 10 mm custom-made tinfoil cups. The cups were filled to two-third and the gelatin was allowed to cool down to around 30°C. To compare the spatial distribution of neuropeptides between different sections within or between brains, reproducible positioning of the samples prior to sectioning is required. To achieve this, each isolated brain was pushed with the anterior surface down in warm gelatin close to the bottom of the tinfoil cup. Next, the brain was slowly entirely covered with warm gelatin, after remaining water had been carefully removed with a glass capillary to avoid salt crystal formation during subsequent snap-freezing to −57°C on the cryobar device provided in the cryotom CryoStar NX50 (ThermoFisher Scientific). Appropriate section thickness, cutting angle, and sample cutting temperature are crucial parameters for high quality, reproducible brain tissue sections (e.g. Buchberger et al., 2018; Ly et al., 2019; Yang & Caprioli, 2011). Therefore, we tested different tissue cutting angles (5° to 25°), cutting temperatures (−30°C to −5°C), and brain section thicknesses (10 to 25 µm). The most efficient

neuropeptide detection was achieved in 14 μm brain sections produced with a cutting angle of 10° at −10°C, which was described as the optimal procedure for MSI analysis of cockroach neuroendocrine tissue (Ly et al., 2019). Using these parameters, we sliced the brain into 14 μm thick sections using a CryoStar NX50 and thaw-mounted them on indium tin oxide coated glass slides (ITO slides; Delta Technologies Limited). Dehydrating the samples in a desiccator evacuated to 300 mbar for at least two days prior to the rinsing procedure ($n = 18$) considerably improved the signal to noise ratio for neuropeptide detection in the ant brain sections (see Figure S1). We therefore dehydrated the tissue sections in a desiccator at 300 mbar with a drying agent (blue silica gel) at room temperature in the dark for at least two days until use.

2.5 | Matrix application

• *Direct tissue profiling*: 10 mg/ml 2,5–dihydroxybenzoic acid (DHB, Sigma-Aldrich, Steinheim, Germany) dissolved in 20% acetonitrile/1% FA/79% water (Fluka) or 10mg/ml α-cyano-4-hydroxycinnamic acid (CHCA; Sigma-Aldrich) dissolved in 60% ethanol, 36% acetonitrile, 4% water were used as matrix stock solutions. Dried tissue samples were covered with either 0.1 μl DHB solution or 0.1 μl of a mixture of one part CHCA stock solution and three parts 50% methanol/water using a 0.1–2.5 μl Eppendorf pipette (Eppendorf AB). Only after DHB application, spots were blow-dried with a commercially available hair dryer to form homogeneous crystals.

• *MSI*: Before matrix application, transmitted light-microscopy images of brain sections were acquired using the PALM Robo-software (V.4.6.0.4) on a PALM Microbeam (Zeiss Corporate) as orientation template for subsequent MALDI-MSI experiments. We applied a rinsing pipeline to remove lipids and increase neuropeptide signals followed existing protocols for the honey bee brain (Pratavieira et al., 2018; Pratavieira et al., 2014) or cockroach RCC sections (Ly et al., 2019) with slight modifications. The best coverage of neuropeptides detection from ant brain sections was obtained by rinsing with 70% ethanol followed by absolute ethanol for 20 s respectively. After each rinsing step, the ethanol was immediately removed by applying a constant compressed air flow for 30 s, which resulted in an additional improvement of neuropeptide detection by a more homogeneous matrix crystal formation afterwards (Figure S2). After the rinsing procedure, samples were dried again using 300 mbar vacuum for 30 min in a desiccator at room temperature in darkness to maximize the solvent removal before matrix application. Matrix application was performed as described by Ly et al., 2019 with slight modifications. In our experiments, the best results were obtained using 5 mg/ml CHCA dissolved in 50% acetonitrile and 1% FA. Matrix coating was performed at a velocity of 900 mm/min, a Z-position of 25 mm, 7 layers with a layer dependent flow rate (layer 1:10 μl/min, layer 2:20 μl/min, layer 3:40 μl/min, layer 4–7:60 μl/min) using a SunCollect Sprayer (SunChrom

GmbH). All settings were adjusted using the SunCollect V. 1.7.52 software package.

2.6 | MALDI-TOF MS

Mass spectra were acquired manually using an ultrafleXtreme TOF/TOF mass spectrometer (Bruker Daltonik GmbH) in reflector positive ion mode in a mass range of 600–10,000 Da. Instrument settings were optimized for the mass range of 600–4,000 Da and 3,000–10,000 Da respectively. Proteins or peptide with a predicted ion mass above 10,000 Da were not analyzed in this study. For calibration, the following synthetic peptide mixture was used: proctolin, *Drosophila melanogaster* (Drm)- sNPF-1[4–11], *Locusta migratoria* periviscerokinin-1 (PVK-1), *Periplaneta americana* (Pea)-FMRFa-12, *Manduca sexta* allatotropin (AT), Drm-IPNa, Pea-SKN and glucagon for the mass range at *m/z* 600–4,000 and a mixture of glucagon, bovine insulin-A, and ubiquitin for the mass range at *m/z* 3,000–10,000 was used. Laser fluency was adjusted to provide an optimal signal-to-noise ratio. The obtained data were processed using FlexAnalysis V.3.4 software package. MS/MS was performed with LIFT technology. LIFT acceleration was set at 1 kV. The number of laser shots used to obtain a spectrum varied from 2,000 to 20,000, depending on ion signal quality. For MS/MS experiments, we also used an ABI 4,800 proteomics analyzer (Applied Biosystems). MS/MS fragment spectra were acquired manually in gas-off mode and processed and handled using DataExplorer V.4.10 software package. Peptide identities were verified by comparison of masses of theoretical (http://prospector.ucsf.edu) and experimentally obtained fragments.

2.7 | MALDI-TOF MSI

MALDI-MSI data were acquired in reflector positive ion mode either on the ultrafleXtreme TOF/TOF mass spectrometer or on a rapifleX TOF/TOF Tissuetyper mass spectrometer (both Bruker Daltonik GmbH). Settings for imaging analysis by ultrafleXtreme instrument were: *m/z* 600–4,000 detection range, 2 kHz Bruker smartbeam-II laser with a laser repetition rate of 1,000 Hz, 1,500 shots per spot, a 15 μm laser-spot size (laser focus diameter setting small) and a 15 μm lateral step size. Recordings using rapifleX instrument are set as following: mass range at m/z 600–3,200, 500 laser shots were accumulated using a Smartbeam 3D Nd:YAG (355 nm) at a frequency of 5,000 Hz and a sample rate of 1.25 GS/s with baseline subtraction (TopHat) during acquisition. The instrument was calibrated using peptide calibration standard II (Bruker Daltonik GmbH) spotted onto the matrix-coated ITO glass slide, taking care that the spot did not obscure the tissue. Ion images were generated using SCiLS Lab MVS software version 2020a (RRID:SCR_014426, Bruker Daltonik GmbH) with the data normalized to the total ion count (TIC). To allow for better comparison between preparations, we used only brain sections that were not

damaged and originated from nearly the same cutting level within each brain. We only analyzed sections of the anterior brain regions between the mushroom bodies (MB) and the central bodies (CB). More posterior brain sections were excluded in subsequent analyses. Raw data (Bruker DAT files) were uploaded and preprocessed in SCiLS Lab and underwent spatial-segmentation analysis using a bisecting-k-means with correlation as distance measure (Trede et al., 2012). The default pipeline was used with the following modifications: weak denoising and an accuracy of mass matching for peptide assignment at $\pm0.05\%$. The lower indication limits for neuropeptide distributions were manually adjusted according to varying strengths of ion signal intensities of different neuropeptides to exclude baseline noises. Overall mass spectra of brain sections were generated with Bruker flexImaging V. 3.4. software package. Mass spectra of individual spots were analyzed with Bruker flexAnalysis V. 3.4. software package.

2.8 | Quadrupole Orbitrap MS Coupled to Nanoflow HPLC

Before injecting the samples into the nanoLC system, extracts were desalted using self-packed Stage Tip C18 (IVA Analysentechnik e.K.) spin columns (Rappsilber et al., 2007). For analysis, peptides were separated on an EASY nanoLC 1,000 UPLC system (Thermo Fisher Scientific) using RPC18 columns 50 cm (fused Silica tube with ID 50 ± 3 μm, OD 150 ± 6 μm, Reprosil 1.9 μm, pore diameter 60 Å, Dr. Maisch, Ammerbuch-Entringen) and a binary buffer system (A: 0.1% FA, B: 80% ACN, 0.1% FA) as described for *Cimex* samples (Predel et al., 2018). Running conditions were as follows: linear gradient from 2% to 62% B in 110 min, 62–75% B in 30 min, and final washing from 75% to 95% B in 6 min (45°C, flow rate 250 nl/min). Finally, the gradients were re-equilibrated for 4 min at 5% B. The HPLC was coupled to a Q-Exactive Plus (Thermo Scientific) mass spectrometer. MS data were acquired in a top-10 data-dependent method dynamically choosing the most abundant peptide ions from the respective survey scans in a mass range of 300–3,000 m/z for HCD fragmentation. Full MS^1 acquisitions ran with 70,000 resolution, with automatic gain control target (AGC target) at 3e6 and maximum injection time at 80 ms. HCD spectra were measured with a resolution of 35,000, AGC target at 3e6, maximum injection time at 240 ms, 28 eV normalized collision energy, and dynamic exclusion set at 25 s. The instrument was run in peptide recognition mode (i.e. from two to eight charges), singly charged and unassigned precursor ions were excluded. Raw data were analyzed with PEAKS Studio 10.5 (BSI). Neuropeptides were searched against an internal database comprising *C. nodus* neuropeptide precursor sequences with parent mass error tolerance of 0.1 Da and fragment mass error tolerance of 0.2 Da. Setting enzymes: none was selected because samples were not digested. The false discovery rate (FDR) was enabled by a decoy database search as implement in PEAKS 10.5. Following posttranslational modification (PTM) were selected: C-terminal amidation as fixed

PTM and oxidation at methionine, N-terminal acetylation, pyroglutamate from glutamine, pyroglutamate from glutamic acid, sulfation of tyrosine, serine, and threonine, as well as disulfide bridges as variable PTMs. In each run a maximum of three variable PTMs per peptide were allowed. Fragment spectra with a peptide score (−10 lgP) equivalent to a *p*-value of ∼1%, were manually reviewed.

2.9 | Immunohistochemistry

Brain sections were prepared as described above and fixated with 4% formaldehyde in 0.1 M phosphate-buffered saline (PBS) overnight at 4°C. After fixation, the sections were rinsed with PBS (3 × 10 min) and pre-incubated in PBS, containing 2% normal goat serum (NGS, Jackson ImmunoResearch Laboratories) for one hour at room temperature. Subsequently, the brain sections were incubated in tachykinin-related peptide antiserum (rabbit anti-LemTKRP-1, kindly provided by Dick Nässel, RRID: AB_2315469) at a concentration of 1:2,500 diluted in PBS with 0.2 Triton-X100, 2% NGS and 0.02% NaN_3 for two hours at room temperature. Afterwards, brain sections were rinsed with 0.1 M PBS three times for 10 min and finally incubated in a mixture of goat anti-rabbit Alexa Fluor 488 (RRID:AB_143165, Thermo Fisher Scientific) at a concentration of 1:250 and CF 633 phalloidin (Catalogue number: 00046; BIOTREND Chemikalien) at a concentration of 1:200 diluted in 0.1 M PBS, containing 1% NGS, as secondary antisera for two hours at room temperature. Phalloidin was used to label filamentous actin (F-actin) (Dancker et al., 1975) in neurons throughout the ant brain, which helps to delineate synaptic neuropils and neuronal fiber tracts in the brain (Habenstein et al., 2020). Then, the samples were rinsed in 0.1 M PBS two times for 10 min and transferred into 60% glycerol in PBS for 30 min at room temperature. Finally, the brain sections were mounted in 80% glycerol in 20% PBS on microscopic slides and coverslips were sealed with nail polish.

2.9.1 | Confocal laser scanning microscopy

Samples were scanned as image stacks with an optical thickness of 0.5–1.5 μm at a resolution of 1,024 × 1,024 pixels using a Leica TCS SP2 AOBS confocal laser-scanning microscope equipped with a 10.0 × 0.4 NA objective (Leica Microsystems AG). Alexa Fluor 488 was excited at 488 nm using an argon/krypton laser and CF 633 phalloidin was excited at 633 nm using a diode laser. Each slice of the stack was scanned 3–4 times and averaged to reduce background noises. Serial optical sections were processed with Fiji (RRID:SCR_002285, ImageJ 1.50e, Wayne Rasband; NIH], Schindelin et al., 2012). In double stained preparations, the different channels were merged with the use of pseudocolors. The final figures were exported and processed to adjust brightness and contrast using CorelDraw Graphics Suite X8 (V. 18.0.0.448; Corel Corporation).

3 | RESULTS

3.1 | Transcriptomics

The transcriptome of *C. nodus* brain tissues (*n* = 4) was assembled into contigs by Trinity followed by BLAST searches using known neuropeptide prepropeptide genes from different insects (Hummon et al., 2006; Liessem et al., 2018; Predel et al., 2010; Schmitt et al., 2015, 2017). In total, a set of 49 *C. nodus* prepropeptide sequences subdivided into 30 complete neuropeptide genes, 7 complete neuropeptide-like genes and, 11 complete, and 1 non-complete protein hormone gene were yielded that likely originate from 42 different genes (Table 1, Figure S3). For the genes encoding agatoxin-like peptide (ALP), CAPA/PVKs, neuropeptide-like precursor-1 (NPLP-1), CCHamide-1, CCHamide-2, and insulin-like peptide-2 (ILP-2), alternatively spliced mRNAs were found. Orthologs of further neuropeptide precursors included in the BLAST search (adipokinetic hormone/corazonin-related peptide [ACP], myoinhibitory peptide [MIP], Ast-C, EFLamide, calcitonin-A, B, natalisin/WAARamide, RYamide, proctolin, insect kinin, HanSolin, RFLamide, and tryptopyrokinin) were not found, neither in the assembled transcriptome data nor by searching in the transcript raw data using homolog insect peptide sequences (see Table 1).

3.2 | Neuropeptidomics

3.2.1 | Brain extract analysis by Q Exactive Orbitrap MS for peptide identification

For chemical identification of transcriptome-predicted peptides and additional precursor peptides (PP), we used the *C. nodus* precursor sequences as database and analyzed brain extracts by ESI-Q Exactive Orbitrap MS followed by PEAKS 10.5 software package. This resulted in sequence identification of products from 16 genes encoding single neuropeptides or neuropeptide-like molecules (adipokinetic hormone [AKH], ALP, AT, allatostatin-CCC [Ast-CCC], calcitonin-like diuretic hormone-31 [DH-31], corticotropin releasing factor-like diuretic hormone [DH-44], CCHamide-2$_a$, Crz; IDL-containing peptide [IDL], ITG-like peptide [ITG], ion transport peptide [ITP], ITP-like, myosuppressin [Ms], pigment dispersing factor [PDF], sNPF, SIFamide), and peptides from nine genes containing multiple copies (Ast-A, CAPA-PVK, extended FMRFamides, NPLP-1, NVP-containing peptide [NVP], orcokinin [Orc], pyrokinin [PK], sulfakinin [SK], TK; see Table 2, Figure S4). We also identified five novel peptides in the brain extracts using de novo sequencing algorithms provides in PEAKS 10.5 software. These peptides show no sequence similarities to known neuropeptides or neuropeptide-like molecules in insects. Consequently, we used NBCI Protein BLAST search against the novel identified peptide sequences which revealed sequence matches to peptides encoded on the uncharacterized protein precursor of various different ant species such as *Solenopsis invicta* (protein LOC105202364; Accession No. XP_011169138.1), *Formica*

exsecta (protein LOC115241177; Accession No. XP_029672667.1), *Camponotus floridana* (protein LOC105254232; Accession No: EFN65144) or *Lasius niger* (protein RF55_8265; Accession No. KMQ91825.1 (Figure S5). Additionally, we found a high sequence similarity between the novel *C. nodus* protein precursor with a protein precursor predicted as stress-response protein in the ant *V. emeryi* (Accession No. XP_011877808). However, this record is predicted by automated computational analysis and derived from a genomic sequence (NW_011967229.1) annotated using gene prediction method: Gnomon from the *V. emeryi* genome, without any functional evidence in stress regulation in the ant. Recently, a neuropeptide gene designated as PaOGS36577 was described in the cockroach *P. americana* by genomics and peptidomics-based strategies, however, without any functional evidence or information about the distribution of the encoded peptides within the brain (Zeng et al., 2021). As tribute for the first evidence of product processing from theses protein precursors within the brain in the ant *C. nodus*, we named the novel peptides Fliktin (Flik) after the impulsive and clumsy inventor ant Flik from the animation movie A Bug´s Life.

3.2.2 | Direct tissue profiling by MALDI-TOF MS

We analyzed several brain areas, portions of the GNG, and the retrocerebral complex (RCC), a peripheral neurohormone storage and release site of insects, which is connected to the brain. The primary objectives were (a) to localize peptides identified by Q Exactive Orbitrap MS experiments to defined brain areas or the RCC, and (b) to find further neuropeptides in the mass range 600–10,000 Da (Table S1,S2) which could not be identified by brain extract MS analysis. Representative mass spectra of the different neuronal regions are shown in Figure 1 and Figure S6, S7. Analysis of portions of the *pars intercerebralis* (PI, *n* = 12), the median protocerebral region in the insect brain where mainly neurosecretory cells are located, revealed the presence of products from 27 genes (Table S1). The most abundant peptides originated from seven neuropeptide genes (*ast-A*, *ast-CCC*, *crz*, *ms*, *snpf*, *orc*, *tk*), two neuropeptide-like genes (*nplp-1*, *nvp*) and one protein hormone gene (*itg*). In addition, ion signals of the novel Flik peptides could also be detected (Figure 1a, Table S1). Potential bioactive molecules produced in the PI are transported via the *nervi corporis cardiaci* (NCC-1) to the RCC. The RCC consists of both nervous and endocrine structures. Mass spectrometrydata obtained from RCC preparation (*n* = 15) revealed ion signals of products from 19 genes (Table S1). The most distinct ion signals mass-matched peptides encoded by the genes *alp*, *ast-CCC*, *crz*, *dh-44*, *ms*, *nvp*, and *flik* (Figure 1b,c). Subsequent fragmentation experiments confirmed the peptide sequences of AKH (as sodium adduct AKH [M + Na]$^+$: *m/z* 1,141.6) Crz (*m/z* 1,369.8), Ast-A-6 (*m/z* 1,427.8), ALP-1$_{a/b}$ (*m/z* 4,861.1), Ast-CCC (*m/z* 1,650.8), extended FMRFa-3 (*m/z* 1,222.6), TK-2 (*m/z* 1,039.5), TK-3 (*m/z* 1,217.6), and TK-4 (*m/z* 1715.9) (Figure S4). Direct profiling of the MB (*n* = 4), centers for learning and memory in insects, confirmed the presence of products from 17 genes (Table S1), with peptides of six genes (*ast-A*, *itg*, *idl*, *nplp-1*, *nvp*, and *tk*)

TABLE 1 Prepropeptide genes for neuropeptides, neuropeptide-like molecules, and protein hormones identified in the transcriptome of *Cataglyphis nodus* brain. Different transcripts are marked with subscript characters (*e.g.*, CCHamide-1$_a$, CCHamide-1$_b$)

Designation	Source	Accession	Complete
Neuropeptide genes			
Adipokinetic hormone	TRINITY_DN1080_c0_g1_i1	MN996797	+
Allatotropin	TRINITY_DN31792_c0_g1_i1	MN996792	+
Allatostatin-A	TRINITY_DN14240_c0_g1_i1	MN996769	+
Allatostatin-CC	TRINITY_DN13459_c0_g1_i1	MN996793	+
Allatostatin-CCC	TRINITY_DN10970_c0_g1_i1	MN996771	+
Arginine–vasopressin-like peptide/ Inotocin	TRINITY_DN26862_c0_g1_i1	MN996787	+
Calcitonin-like diuretic hormone−31	TRINITY_DN13546_c0_g1_i1	MN996801	+
CAPA$_a$/Periviscerokinin	TRINITY_DN8747_c0_g1_i1	MN996766	+
CAPA$_b$/Periviscerokinin	TRINITY_DN8747_c0_g2_i1	MN996767	+
CCHamide−1$_a$	TRINITY_DN15956_c0_g1_i1	MN996776	+
CCHamide−1$_b$	TRINITY_DN15956_c0_g1_i4	MN996777	+
CCHamide−2$_a$	TRINITY_DN10059_c0_g1_i1	MN996783	+
CCHamide−2$_b$	TRINITY_DN10059_c0_g1_i2	MN996784	+
CNMamide	TRINITY_DN10563_c0_g1_i2	MN996802	+
Corazonin	TRINITY_DN31041_c0_g1_i1	MN996775	+
Corticotropin releasing factor-like diuretic hormone	TRINITY_DN15881_c0_g1_i1	MN996782	+
Crustacean cardioactive peptide	TRINITY_DN31220_c0_g1_i1	MN996773	+
Ecdysis triggering hormone	TRINITY_DN2946_c0_g1_i1	MN996768	+
Elevenin	TRINITY_DN15212_c0_g1_i1	MN996762	+
Extended FMRFamide	TRINITY_DN14605_c0_g1_i1	MN996772	+
Myosuppressin	TRINITY_DN14195_c0_g1_i1	MN996806	+
Neuropeptide F	TRINITY_DN14055_c0_g1_i1	MN996770	+
Orcokinin	TRINITY_DN14752_c0_g1_i1	MN996788	+
Pigment dispersing factor	TRINITY_DN23971_c0_g1_i1	MN996807	+
Pyrokinin	TRINITY_DN9819_c0_g1_i1	MN996789	+
short neuropeptide F	TRINITY_DN16538_c0_g11_i1	MN996779	+
SIFamide	TRINITY_DN5040_c0_g2_i1	MN996785	+
Sulfakinin	TRINITY_DN9919_c0_g1_i1	MN996781	+
Tachykinin-related peptide	TRINITY_DN16581_c0_g1_i2	MN996780	+
Trissin	TRINITY_DN14132_c0_g2_i1	MN996805	+
Neuropeptide-like genes			
Agatoxin-like-peptide−1$_a$	TRINITY_DN14927_c0_g1_i1	MN996764	+
Agatoxin-like-peptide−1$_b$	TRINITY_DN14927_c0_g2_i1	MN996765	+
Fliktin	TRINITY_DN18124_c1_g1_i2	MN996812	+
Neuropeptide-like precursor−1$_a$ (NPLP−1$_a$)	TRINITY_DN18383_c1_g1_i2	MN996809	+
Neuropeptide-like precursor−1$_b$ (NPLP−1$_b$)	TRINITY_DN18383_c1_g1_i3	MN996810	+
Neuropeptide-like precursor−1$_c$ (NPLP−1$_c$)	TRINITY_DN18383_c1_g1_i1	MN996808	+
NVP-like peptides	TRINITY_DN18939_c7_g1_i1	MN996799	+
Protein hormone genes			
Bursicon-*alpha*	TRINITY_DN17815_c6_g2_i1	MN996790	+
Bursicon-*beta*	TRINITY_DN17815_c2_g1_i1	MN996813	(+)
Eclosion hormone	TRINITY_DN20318_c0_g1_i1	MN996774	+

(Continues)

TABLE 1 (Continued)

Designation	Source	Accession	Complete
IDL-containing peptide	TRINITY_DN12956_c0_g8_i1	MN996800	+
ITG-like peptide	TRINITY_DN17809_c3_g1_i1	MN996791	+
Insulin-like peptide−1	TRINITY_DN18145_c0_g1_i1	MN996811	+
Insulin-like peptide−2_a	TRINITY_DN16229_c0_g1_i2	MN996804	+
Insulin-like peptide−2_b	TRINITY_DN16229_c0_g1_i1	MN996803	+
Ion transport peptide-like	TRINITY_DN12575_c0_g1_i2	MN996796	+
Ion transport peptide	TRINITY_DN12575_c0_g1_i1	MN996795	+
Neuroparsin	TRINITY_DN863_c0_g1_i1	MN996794	+
Prothoracicotropic hormone	TRINITY_DN5171_c0_g1_i1	MN996778	+

Note: Precursor sequences are listed in Supporting Information S3, which also consider partial sequences (+). Precursor sequences were annotated and submitted to GenBank ((BioProject: PRJNA602618, BioSample: SAMN13899910, Sequence Read Archive (SRA): SRP10955559).

showing the highest ion signal intensities (Figure 1d). Measurements of the optic lobe (OL) region ($n = 8$), which contains the first synaptic relay for visual information and parts of the central circadian clock in insects, exposed peptide precursor products from 17 genes (Table S1). The most prominent ion signals belonged to putative neuroactive substances encoded by the *ast-a-*, *itg-*, *idl-*, *tk-*, *nplp-1-*, *orc*, *pdf-*, and *sifamide* gene (Figure 1e). Analysis of the antennal lobe (AL, $n = 10$), the first synaptic relay of olfactory information, revealed the presence of neuropeptides from 18 different precursor genes (Table S1) with prominent ion signals for products of *snpf-*, *tk- dh-31- and nplp-1-* gene (Figure 1f). Furthermore, the predicted ion mass of trissin (m/z 3,024.3), CCHamide-$1_{a,b}$, 2_b, CCAP, elevenin and PTTH-PPs were detected by mass matches (see Table 2). Distinct ion signal intensities corresponding to extended FMRFa were observed in preparations of the GNG ($n = 6$) which allowed the validation of the peptide sequence of extended FMRFa-3 (Figure S6, S7). Transcriptome-predicted sequences for bursicon-alpha, bursicon-beta, EH, ETH, ILP-$2_{a,b}$, NP, and neuropeptide F were neither identified by Q Exactive Orbitrap MS nor by direct tissue profiling. In line with the lack of respective transcripts in our *C. nodus* brain transcriptomic data set, peptidomics did not support the presence of ACP, MIP, Ast-C, calcitonin-A, B, HanSolin, natalisin/WAARamides, RFLa, RYamide, proctolin, insect kinin, and tryptopyrokinin.

3.3 | MALDI-TOF MSI

3.3.1 | Sample preparation and reproducibility of neuropeptide detection in *C. nodus* brain sections

In the last decade, MALDI-TOF MSI has moved into the center stage for untargeted analysis of the spatial distribution of molecule species such as neuropeptides in tissue samples. The availability of more sensitive, robust and precise mass spectrometers improved the detection of putative neuropeptides directly from tissue sections. As a first step to uncover potential functions of neuropeptides in age-related polyethism and during distinct behavioral stages in ants, we

optimized available MSI protocols (*e.g.* Chen & Li, 2010, Pratavieira et al., 2014, Ly et al., 2019) for neuropeptide detection in the *C. nodus* brain to gain comprehensive information of the spatial distribution of these signaling molecules in the tiny ant brain. We evaluated different experimental steps including sample preparation, tissue embedding material, tissue thickness, tissue rinsing procedure, tissue storage, matrix composition and matrix application tools for *C. nodus* brain sections as described in the experimental procedures (see 2.4, 2.5 and 2.7).

In our study, we used two commercially available mass spectrometer for MSI analysis. To evaluate the reproducibility of our optimized MSI for neuropeptide detection, we compared twelve brain sections analyzed either on an ultrafleXtreme (nine brain sections) or rapifleX (three brain sections) instrument based on the detectable number of neuropeptides as well as the quality of ion signal intensities. Resulting overall mass spectra from all 12 brain section revealed good signal to noise ratios, high quality ion signal intensities for the detection of putative bioactive mature neuropeptides and a nearly identical number of detectable neuropeptides per brain slide (Figure S8).

3.3.2 | Spatial distribution of neuropeptides in the ant brain: MALDI- MSI

Among the characterized *C. nodus* brain neuropeptides, we were able to visualize the spatial distribution of 35 peptides encoded on 16 precursor genes (*ast-A, at, capa, crz, dh-31, fmrf, idl, inotocin, itg, ms, nplp-1, nvp, orc, snpf, tk, flik*) in 14 μm thin sections using our optimized MALDI- MSI protocol. Figure 2 shows typical peptide ion maps in brain sections. Signals for Ast-A, IDL, Flik, inotocin, Orc, and TK were most prominent in the MBs, whereas products from the *capa* and the *dh-31* genes were almost exclusively detectable in the ALs in these sections. Furthermore, ion maps of Flik, ITG, NPLP-1, TK, Orc, and sNPF revealed distinct peptide presences in the AL. Dorsal to the ALs, Ast-A, IDL, ITG, FMRFa, myosuppressin, NPLP-1, NVP, Flik, sNPF, Orc, and TK were mapped with distinct ion

TABLE 2 Alphabetic list of mature neuropeptides, neuropeptide-like, protein hormones, and precursor peptides (PP) of *C. nodus* brain and retrocerebral complex (RCC) samples analyzed using three different mass spectrometrical approaches

Designation	Sequence	m/z [M + H]$^+$,	MS	MS^b	MSI
Adipokinetic hormone (AKH)					
AKH	pQLNFSTGWGQ-NH$_2$	1,119.55	+	+	–[*]
Agatoxin-like-peptide$_a$ (ALP$_a$)					
ALP$_a$	ACIRRGGNCDHRPKDCCYSSSCRCNLWGSNCQCQRMGLFQ KW-NH$_2$	4,861.11	+	–	–[a]
Agatoxin-like-peptide$_b$ (ALP$_b$)					
ALP$_b$	ACIRRGGNCDHRPKDCCYSSSCRCNLWGSNCQCQRMGLFQ KW-NH$_2$	4,861.11	+	–	–[a]
Allatotropin (AT)					
AT	GFKPEYISTAIGF-NH$_2$	1,428.75	+	(+)	+
Allatostatin-A (AST-A)					
Ast-A-1	LPLYNFGI-NH$_2$	935.53	+	+	+
Ast-A-2	TRPFSFGI-NH$_2$	923.51	+	+	+
Ast-A-3	LRDYRFGI-NH$_2$	1,038.58	+	+	+
Ast-A-4	GGQPFSFGI-NH$_2$	908.46	+	+	–
Ast-A-5	PNDVIGPKYLLSL-NH$_2$	1,427.83	+	–	–
Ast-A-PP-1	AVEEAPSSSLHIPRLNPLSSSLEGYDKPSE-OH	3,209.60	+	+	–
Ast-A-PP-2	AYAYISEY-OH	979.44	+	–	+
Allatostatin-CCC (AST-CCC)					
Ast-CCC	SYWKQCAFNAVSCF-NH$_2$	1,650.73	+	+	–
Ast-CCC-PP	MPTTDTDKDRLLNTVDLIDDDGSIETALINYLFTKQIV-OH	4,297.18	+	–	–[a]
Allatostatin-CC (Ast-CC)					
Ast-CC	GQAKGQVYWRCYFNAVTCF-OH	2,238.04	+	–	–
Arginine–vasopressin-like peptide/Inotocin					
Inotocin	CLITNCPRG-NH$_2$	973.49	+	–	+
Calcitonin-like diuretic hormone-31 (DH-31)					
DH-31	GLDLGLSRGFSGSQAAKHLMGLAAANYAGGP-NH$_2$	2,986.53	+	+	+
DH-31-PP	IPHSHESYWDQQDDMDRDEFLDILSRLSRTVMNRPEMENS -OH	4,892.21	+	(+)	–[a]
DH-31-PP$^{1-28}$	IPHSHESYWDQQDDMDRDEFLDILSRLS-OH	3,447.55	+	(+)	–
DH-31-PP$^{30-40}$	TVMNRPEMENS-OH	1,307.57	+	+	+
CAPA$_a$/Periviscerokinin (PVK)					
CAPA$_a$-PVK-1	SAGLVPYPRI-NH$_2$	1,071.63	+	+	+
CAPA$_a$-PVK-2	ALGMINVPRV-NH$_2$	1,068.63	+	–	+
CAPA$_a$-PK	NTQGQGGYTPRL-NH$_2$	1,290.65	+	+	–
CAPA$_a$-PVK-PP-1(Q)	QKLKAND-OH	816.46	+	+	–
CAPA$_a$-PVK-PP-1 (pQ)	pQKLKAND-OH	799.46	+	+	–
CAPA$_a$-PVK-PP-2	NSEISSISRSE-OH	1,208.58	+	+	+
CAPA$_b$/Periviscerokinin (PVK)					
CAPA$_b$-PVK-1	SAGLVPYPRI-NH$_2$	1,071.63	+	+	+
CAPA$_b$-PVK-2	ALGMINVPRV-NH$_2$	1,068.63	+	–	+
CAPA$_b$-PK	NTQGQGGYTPRL-NH$_2$	1,290.65	+	+	–
CAPA$_b$-PVK-PP-1	SVGQQFESAREGQKLKAND-OH	2092.04	+	–	–
CAPA$_b$-PVK-2-PP-2	NSEISSISRSE-OH	1,208.58	+	+	+

(Continues)

TABLE 2 (Continued)

Designation	Sequence	m/z [M + H]$^+$,	MS	MS^b	MSI
CCHamide-1					
CCHa-1	SCLSYGHSCWGAH-NH$_2$	1,404.57	+	–	–
CCHamide-2$_a$					
CCHa-2$_a$	GGCASFGHSCFGGH-NH$_2$	1,320.52	–	+	–
CNMamide					
CNMa	HGTNTVSYMSLCHFKICNM-NH$_2$	2,182.98	+	–	–
Corazonin (Crz)					
Crz	pQTFQYSRGWTN-NH$_2$	1,369.65	+	+	+
Crz-PP	SEFPSSPEISTAGYERINNGDLNRLKMLIHGSTDEQPLIIHCDFV DKLRNFLQTDNYAPQLHREKGPNLDY-OH	8,170.03	+	–	–^{a}
Corticotropin releasing factor-like Diuretic hormone (DH-44)					
DH-44	IGSLSIVNNLDVLRQRVLLELARRKQEQDLRQIQENRRVLENI -NH$_2$	5,136.93	+	(+)	–^{a}
DH-44-PP-1	APLSSYERRDMSDDGPKIFLLMDERIPELENEILGNDLGSDVTR T-OH	5,107.50	+	–	–^{a}
DH-44-PP-2	SVPGSDAGRIARSGKSRNDRDRPAVSNRIEWIEEDDPLFRGSQ DGRMARVQANELRLL-OH	6,519.33	+	–	–^{a}
Crustacean cardioactive peptide (CCAP)					
CCAP	PFCNAFTGC-NH$_2$	956.39	+	–	–
Ecdysis triggering hormone (ETH)					
ETH-1	DEVPAFFLKIAKMKTLPRV-NH$_2$	2,202.28	–*		
ETH-2	SGRFEDFFYKAEKHIPRI-NH$_2$	2,239.18	–*		
Elevenin					
Elevenin-1	VDCERNPYDRSCRGAQI-OH	1979.90	+	–	–
Elevenin-2	LEQIDQQDVYMDY-OH	1659.72	+	–	–
Extended FMRFamide					
FMRFa-1	SNMGSSFIRF-NH$_2$	1,144.56	+	–	+
FMRFa-2	WKSPDVVIRF-NH$_2$	1,245.71	+	+	–
FMRFa-2$^{3-10}$	SPDVVIRF-NH$_2$	931.54	+	+	–
FMRFa-3	GKNDLNFIRF-NH$_2$	1,222.67	+	+	+
FMRFa-PP-1	SILKDDSSLRIFKESPNEFEYVV-OH	2,715.39	+	(+)	+
FMRFa-PP-2	TDLDDRKEDTESKE-OH	1,680.76	+	(+)	–
FMRFa-PP-3	GQSFDNSALDNEIDSKVSRHPRW-OH	2,658.27	+	(+)	–
Fliktin (Flik)					
Flik-1	SLDAADTPEYYNDLHSF-OH	1957.84	–	+	–
Flik-2	NVNGRYPIGREFGNY-OH	1755.86	+	+	+
Flik-3	LTKRYPVA-OH	947.57	+	+	+
Flik-4	SPRPTQTKLKTTDP-OH	1569.86	+	+	+^{b}
Flik-4$^{1-9}$	SPRPTQTKL-OH	1,027.59	+	+	+
Flik-5	ATFTAGHNTQNQDDEWMLQ-OH	2,206.95	–	+	–
IDL-containing peptide					
IDL	IDLSRFYGHINT-OH	1,435.73	+	+	+
Insulin-like peptide-1 (ILP-1)					
ILP-1-PP	DGYPQFNPK-OH	1,065.50	+	–	–
Ion transport peptide-like (ITP-like)					

TABLE 2 (Continued)

Designation	Sequence	m/z [M + H]+,	MS	MS[b]	MSI
ITP-like-PP	ATLNGHPL-NH2	821.46	+	+	−
Ion transport peptide (ITP)					
ITP-PP	ATLNGHPL-NH2	821.46	+	+	−
ITP	SFFDIQCKGVYDKSIFARLDRICEDCYNLFREPQLHMLCKQDCF STQYFTSCIQALLLEDEKERLQEMVEYL-NH2	8,691.13	+	−	−[a]
ITG-like peptide					
ITG	ITGQGNRLF-OH	1,005.55	+	+	+
Myosuppressin (Ms)					
Ms (pQ)	pQDVDHVFLRF-NH2	1,257.66	+	+	+
Ms (Q)	QDVDHVFLRF-NH2	1,274.66	+	+	+
Ms-PP	AMPLQCNSGFLEELPPRLRKICVAIARIWDAREMNDFVDNREY RENLPRYDSSV-OH	6,394.17	+	−	−[a]
Neuropeptide-like precursor-1 (NPLP-1)					
NPLP-1–1	NVGSLARDFALPK-NH2	1,386.79	+	+	+
NPLP-1–2	HIASVAREYGLPS-NH2	1,398.75	+	+	+[b]
NPLP-1–3	NIGSLARQSMMPLG-NH2	1,473.77	+	+	+
NPLP-1–4	NIASLARYDMLPQN-NH2	1604.82	+	+	+
NPLP-1–5	NVAALARDSSLPY-NH2	1,375.73	+	+	+
NPLP-1–6	YLGSLARNGGYQTVREYDD-NH2	2,176.04	+	+	+
NPLP-1–7	SIASLARNADWPGIV-OH	1569.84	+	+	+
NPLP-1–8	GRMTSGRIIARVLNRH-NH2	1836.06	+	−	+
NPLP-1–9	FSRSPRYLVERS-NH2	1,495.81	+	−	−
NVP-like peptides					
NVP-1	ADQAMKPKS-OH	975.49	−	+	−
NVP-2	TQEMLMFGNQQNRQANAAASESFTSNAE-OH	3,075.35	+	(+)	−
NVP-3	LVSTTQQPVQAQV-OH	1,398.76	+	−	+[b]
NVP-4	SVPFYQEPRF-OH	1,269.63	+	+	+
NVP-5	MQSYDPYSTAQLQLSSQPRSYQYPHRVVY-OH	3,492.66	+	+	−
Orcokinin (Orc)					
Orc-1	GPVQGASNAVQQDTYASPADLAILARYLENRNAGNRNLDGY LLRQT-OH	4,974.52	+	(+)	−[a]
Orc-2	RGLDSLSGATFGEN-OH	1,423.68	+	+	+
Orc-3	YVPLRRFGAISLQPGNFDEIDRSVFDRFS-OH	3,401.74	+	(+)	−
Orc-3[16–29]	NFDEIDRSVFDRFS-OH	1746.81	+	(+)	−
Orc-4	NIDEIDTAFDSFF-OH	1533.67	−	+	−
Orc-5	NFDEIDRAGWSGFV-OH	1612.74	+	+	+
Orc-6	LNNYLADRQ-NH2	1,105.57	+	+	+
Pigment dispersing factor (PDF)					
PDF	NSELINSLLSLPKNMHNA-NH2	1994.05	+	(+)	−
Prothoracicotropic hormone (PTTH)					
PTTH-PP-1	EGPGQVLSIGRWKEQVVAPEFLLDDREDITSNRRNAFFYED-OH	4,640.27	+	−	−[a]
PTTH-PP-2	SFRPEGLGEQV-OH	1,218.61	+	−	−
Pyrokinin (PK)					
PK-1	TTAQEITSGMWFGPRL-NH2	1793.90	+	−	−
PK-2 (Q)	QQTQFTPRL-NH2	1,117.61	+	−	−

(Continues)

TABLE 2 (Continued)

Designation	Sequence	m/z [M + H]+,	MS	MSb	MSI
PK-2 (pQ)	pQQTQFTPRL-NH2	1,100.61	+	+	−
PK-3	GSDEELFSYGDATDRNEIEENDRLLPPIFAPRL-NH2	3,777.84	+	(+)	−
PK-4	RVSWIPSPRL-NH2	1,209.72	+	+	−
PK-PP-1	EYELRETPNGGSNDNRSPSNEFGSCIEGKCT-OH	3,388.45	+	−	−
PK-PP-2 (Q)	QSRSVSRKI-OH	1,060.62	+	−	−
PK-PP-2 (pQ)	pQSRSVSRKI-OH	1,043.62	+	−	−
Short neuropeptide F (sNPF)					
sNPF	SQRSPSLRLRF-NH2	1,345.78	+	−	+
sNPF[4-11]	SPSLRLRF-NH2	974.59	+	+	+
sNPF-PP-1	TENYMDYGEEMAEKTPADNIHEFYRLLLQRNALDNAGFGSIPL EHLMI-OH	5,569.65	+	(+)	−[a]
sNPF-PP-2	SGPHISARDLARPVGAAAGYNDNN-OH	2,423.18	+	(+)	+
SIFamide					
SIFa	YKKPPFNGSIF-NH2	1,296.71	+	+	−
Sulfakinin (SK)					
SK-1	pQQLDDYGHMRF-NH2	1,391.64	+	−	−
SK-2	SNGDDEEYGHSRF-NH2	1511.64	+	+	−
SK-2	SNGDDEEY(S0₃)GHSRF-NH2	1,590.61	−	+	−
Tachykinin-related peptide (TKRP)					
TK-1 (6×)	APMGFQGMR-NH2	993.48	+	+	+
TK-2	TIMGFQGMR-NH2	1,039.52	+	+	+
TK-3	SPFRYFDMR-NH2	1,217.59	+	+	+
TK-4	NPRWELRGMFVGVR-NH2	1715.93	+	+	−
TK-PP-1	VPMGFQDMRE-OH	1,209.54	+	+	−
TK-PP-2	NLIPTSAEHNKLSQRTLMDFQDMRDDKESNAPDIEDNLLHEF E-OH	5,056.37	+	+	−[a]
TK-PP-3	DYLTPDFEDFYFRNE-OH	1970.84	+	(+)	+
TK-PP-4	SLEEVLGEIE-OH	1,117.56	+	−	−
TK-PP-5	AAMNFYGTKE-OH	1,131.51	+	+	−
TK-PP-6	TYVLEYPEDYEKRLLAMGFQGTRGKLKEFPGEWE-OH	4,080.02	+	−	−[a]
TK-PP-6[1-11]	TYVLEYPEDYE-OH	1,420.62	+	−	−
TK-PP-6[14-34]	LLAMGFQGTRGKLKEFPGEWE-OH	2,394.23	+	+	−
TK-PP-7	SLLDEIEELE-OH	1,189.58	+	+	−
Trissin					
Trissin	VSCDQCGRECADICGTRQFRACCFNNM-OH	3,024.20	+	−	−

Note: Direct tissue profiling by MALDI-TOF mass spectrometry (MS) with subsequent MSMS fragmentation experiments and brain tissue extraction analyzed by ESI-Q-TOF MS were used for peptide sequence confirmation (bracket: a part of the peptide amino acid sequence is confirmed). Because of the lack of basic amino acids, AKH is detected as sodium [M + Na]+ and potassium [M + K]+ adducts. MSI was applied for selected neuropeptide spatial distribution within fresh-frozen 14 μm thin brain sections.

[a]Out of detection range in MSI experiments.

[b]Peptide distribution is inferred by mass matches.

*Not produced from neurons of the brain.

intensities. The ion map of Crz showed a unique distribution pattern as only ion signals in the region of the *pars lateralis* (PL), a neuroendocrine center in insects, were found. In the region of the CB, neuropeptides encoded on the *dh-31, itg, myosuppressin, nvp, orc,* and *tk* genes were observed.

Insect neuropeptides are contained either as a single copy (*e.g.* AT, Crz, myosuppressin) or as multiple copies (paracopies, *e.g.* Ast-A, extended FMRFamides, TKs, PKs) within the precursor proteins. In MALDI-TOF mass spectrometric diagrams, the ion signal intensities of paracopies show constant relative patterns which resulted in
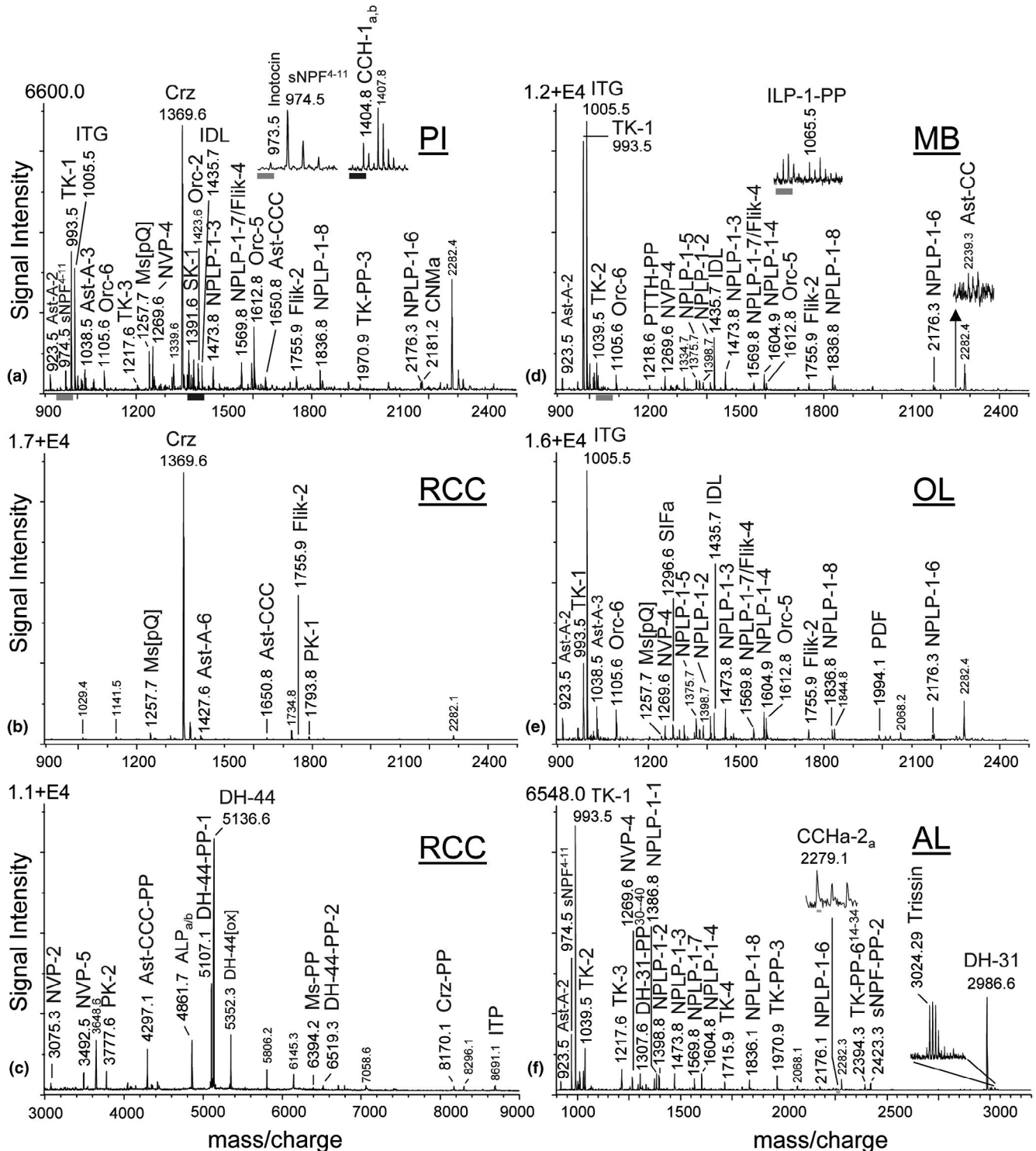
FIGURE 1 Representative MALDI-TOF mass spectra (direct tissue profiling) obtained from preparations of (a) cell population of the *pars interecerebralis* (PI, *n* = 12 samples from 12 brains), (b) the retrocerebral complex (RCC, *n* = 15 samples from 15 animals) in the mass range m/z 900–2,500, (c) the RCC in the mass range m/z 3,000–9,000, (d) a portion of the mushroom body (MB, *n* = 4 samples from 4 brains), (e) an optic lobe (OL, *n* = 8 samples from 8 brains) and (f) an antennal lobe (AL, *n* = 10 samples from 10 brains). Ion signals are marked and represent single charged peptides [M + H]$^+$. Ast-A, allatostatin-A; Ast-CCC, allatostatin-CCC; DH-31, calcitonin-like diuretic hormone-31; DH-44, corticotropin-releasing factor-like diuretic hormone-44; Crz, corazonin; IDL, IDL-containing peptide; ITG, ITG-like peptide; ITP, ion transport peptide; Ms, myosuppressin; TK, tachykinin-related peptide; NVP, NVP-containing peptide; NPLP-1, neuropeptide-like precursor 1; Orc, orcokinin; Flik-fliktin; PDF, pigment dispersing factor; PK, pyrokinin; PP, precursor peptide; sNPF, short neuropeptide F; SK, sulfakinin
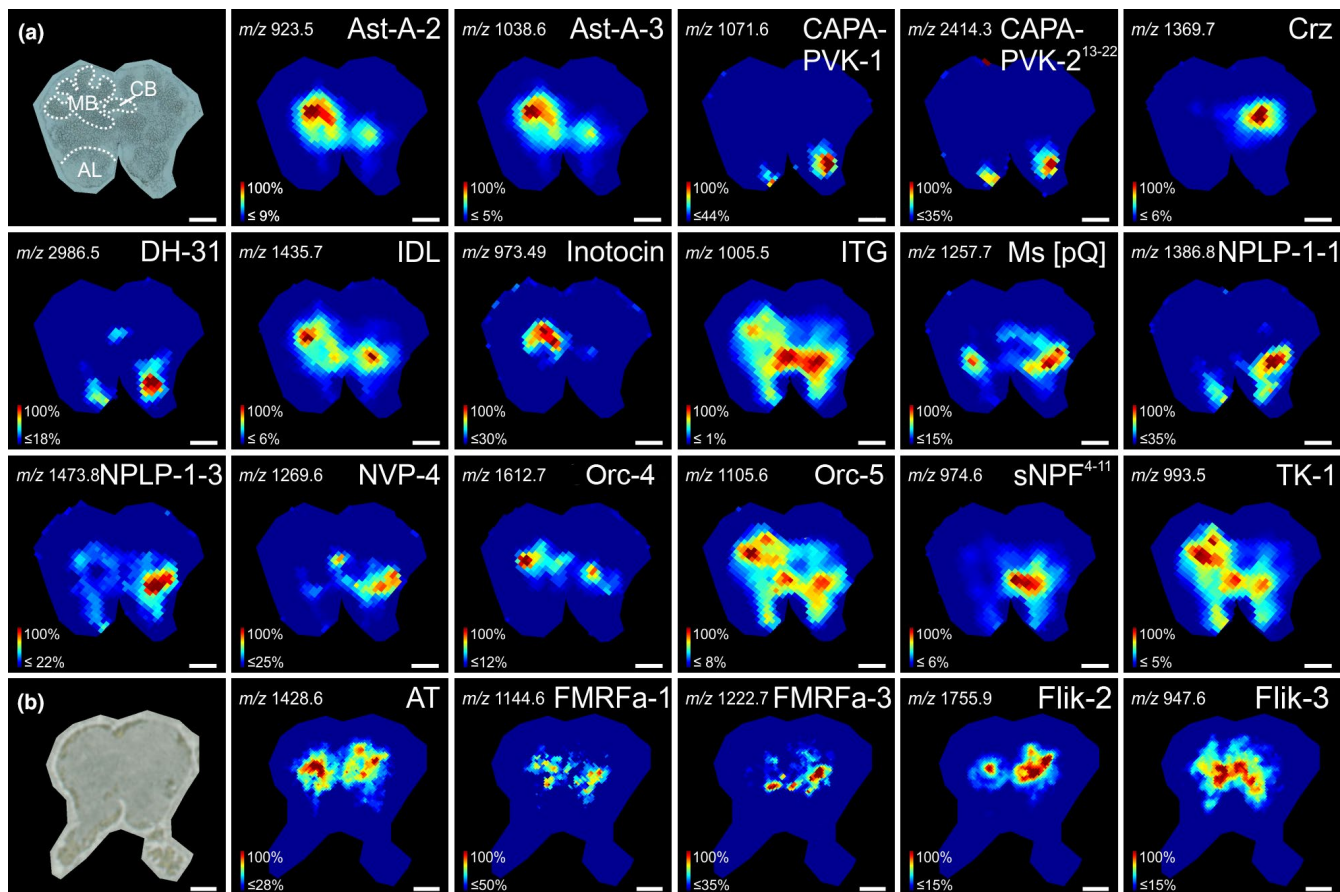
FIGURE 2 MALDI-MSI ion maps show the spatial distribution of 22 peptides from 16 genes in two exemplary ant brain sections recorded using the (a) UltrafleXtreme (first section) and (b) rapifleX MS instrument (second section). The accuracy of mass matching for peptide assignment was settled at ±0.05%. Ast-A, allatostatin-A; AT, allatotropin; DH-31, calcitonin-like diuretic hormone-31; Crz, corazonin; CAPA-PVK, CAPA/periviscerokinin; FMRFa, extended FMRFamides; IDL, IDL-containing peptide; ITG, ITG-like peptide; ITP, ion transport peptide; Ms myosuppressin; TK, tachykinin-related peptide; NVP, NVP-containing peptide; NPLP-1, neuropeptide-like precursor 1; Orc, orcokinin; Flik, fliktin; PP, precursor peptide; sNPF, short neuropeptide F. Scale bars = 200 μm

similar spatial distributions in imaging ion maps as shown exemplarily for TKs in Figure 3a. The spatial distribution of three mature neuropeptides (TK-1, -2, -3) and one precursor protein (TK-PP-3), all encoded on the *tk*-gene, were detected in a single brain section. Each *tk*-gene product has a different amino acid sequence (Table 2) which resulted in a different molecule ionization efficiency in MALDI-TOF MS and, thus, different ion signal intensities in resulting mass spectra (Figure 3b,c). Ion maps of TK-4 and TK-PP-1, -2, -4 to -8 were not visualized in this section, likely because their ion intensities were either too low or the ion mass (TK-PP-2, *m/z* 5,056.4) was out of the detection range.

To interpret the large dataset resulting from each single brain imaging analysis, we applied bisecting k-means segmentation clustering using SCILS Lab. The result of the segmentation analysis is a binary hierarchical tree containing nested sub regions, each defined by a unique composition of different ion signals within the mass spectrum. A representing spatial segmentation analysis of a single ant brain section is shown in Figure 4. The analyzed ants MSI dataset could be compartmentalized into certain clusters which enabled the assignment of subdivided regions of the protocerebrum, the PL

(left side) and the MB (right side) as well as the neuropil region of the deutocerebrum, the ALs.

3.3.3 | Spatial distribution of neuropeptides in the ant brain: MALDI-MSI and immunostaining

The immunostaining pattern of TK is well-characterized for the brain of *Cataglyphis* (Schmitt et al., 2017). To evaluate the precision of our MALDI-MSI neuropeptide data set, we therefore performed immunostainings against TK combined with MALDI-MSI in consecutive brain sections (Figure 5). To visualize neuroanatomical landmarks in the brain, we co-stained the brain sections with fluorophore-conjugated phalloidin as a general label for neuronal tissue that helps to delineate neuropil regions and fiber connections in brain regions that are devoid of cell bodies. TK-*like* immunoreactivity was found throughout the brain sections, with very distinct labeling in the CB, the MB, and the AL (Figure 5 [S1, S3, S5]) as previously described (Schmitt et al., 2017). MALDI-MSI and TK-*like* immunoreactivity data illustrated very well the
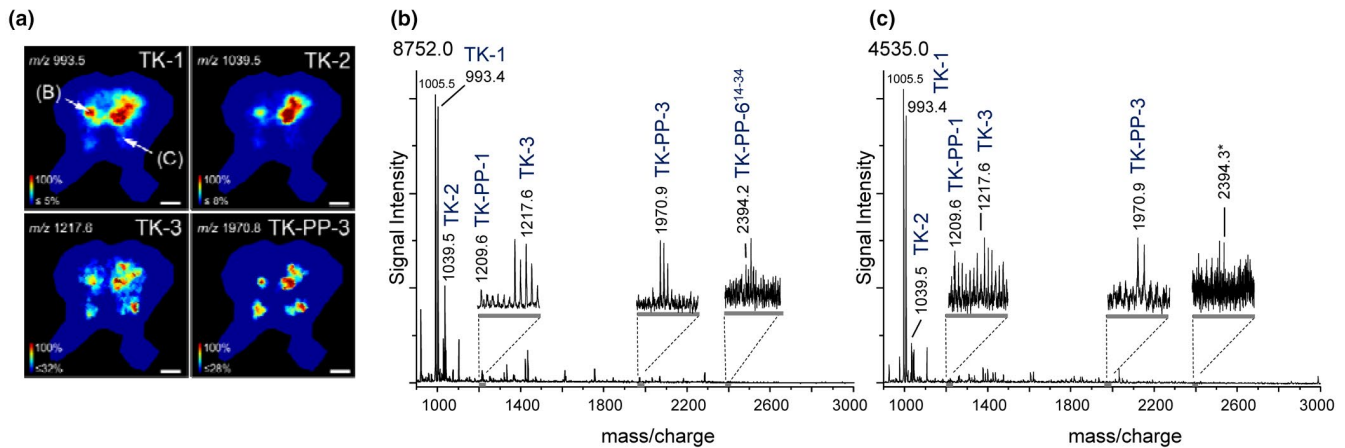
FIGURE 3 MALDI-MSI ion maps demonstrating the spatial distribution of products from *tachykinin-related peptide* (*tk*) gene analyzed from a *C. nodus* brain section (thickness: 14 μm) recorded using the rapifleX MS instrument. The *tk*-gene encodes four different tachykinin-related peptides (TK) and eight TK-PPs. (a) Ion signal intensity of three TKs (TK-1, -2, -3) and TK-PP-3 was sufficient to be visualized in these MALDI-MSI spectra. The accuracy of mass matching for peptide assignment was settled at ±0.05%. Minimum intensity was defined individually for each ion of interest to ignore smaller peaks in the baseline which could be cause in false positive ion distribution. Scale bar: 200 μm. (b, c) Mass spectra obtained by MSI showing the relative signal intensities of TK paracopies processed from the *tk*-gene at different neuronal regions of the brain. The absence of an ion signal representing TK-PP-6$^{14-34}$ in (c) (marked with an asterisk) is a result of the lower signal intensity of TK paracopies at this spot relative to the analyzed region in B. The analyzed spots are indicated in (a) by white arrows
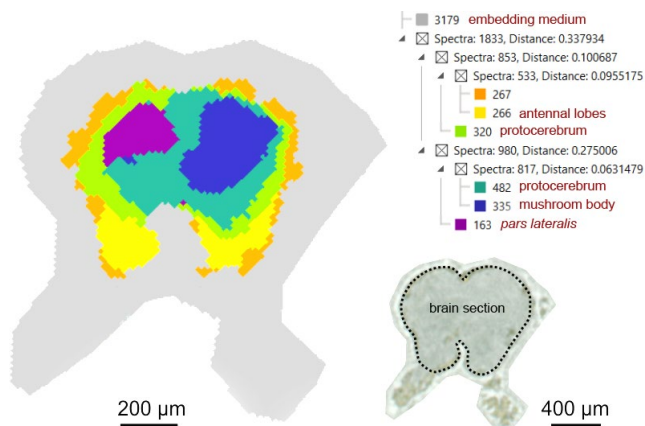

FIGURE 4 Spatial segmentation analysis based on MS imaging data measured from a single brain section using the rapifleX MS instrument. The color-coded levels in the segmentation dendrogram reveal different regions of the protocerebrum including the right neuropil area of the mushroom body and the lateral neurosecretory area, the *pars lateralis* as well as the deutocerebral neuropil region, the antennal lobes. The statistical evaluation of our MSI data showing division of *C. nodus* brain in different neuropil brain regions, which is consistent with the recently described neuroanatomical organization of the *Cataglyphis* brain (Habenstein et al., 2020)

spatial distribution of TKs throughout consecutive brain sections, as illustrated by ion maps for TK-1 (Figure 5 [S2, S4, S6]). Slight mismatches between MALDI-MSI and the immunostaining data are attributable to the different brain regions in consecutive section as well as to the nature of evaluation methods underlying the two distinct methods (MALDI-MSI and immunohistochemistry). The immunohistochemical images (Figure 5 [S1, S3, S5]) do not

display relative differences of the TK abundances. Consequently, TK occurs in bright green wherever the antibody binds in a certain quantity. In contrast, MALD-MSI images (Figure 5 [S2, S4, S6]) display the relative signal intensity of the analyte throughout the brain sections. For instance, we detected TK also in the AL using MALDI-MSI. However, the detected expression (ion signal intensity) of TK was considerably lower than in other parts in the brain. We found the highest TK levels in the mushroom body (indicated in red) whereas the TK level in the AL was in most cases only 0.1%–10% (indicated in dark to light blue) of it. Throughout consecutive serial sections of the MB, a slightly asymmetric distribution of TK-1 and TK-*like* immunoreactivity between the right and the left cerebral hemisphere was observed in more posteriorly located brain layers. Overall, the largely coherent findings using both visualization methods show that the applied MALDI-MSI procedure is suitable to detect and localize neuropeptides at high spatial resolution, even within small subcompartments of the *C. nodus* brain.

4 | DISCUSSION

Our study presents a comprehensive chemical as well as spatial characterization of the peptidome from the small brain of the ant *C. nodus*, obtained by a combination of transcriptomic and different MS approaches (see Table S2).

4.1 | *C. nodus* brain transcriptome

The transcriptome from adult *C. nodus* worker brains revealed 49 precursor proteins belonging to 27 neuropeptides, 4
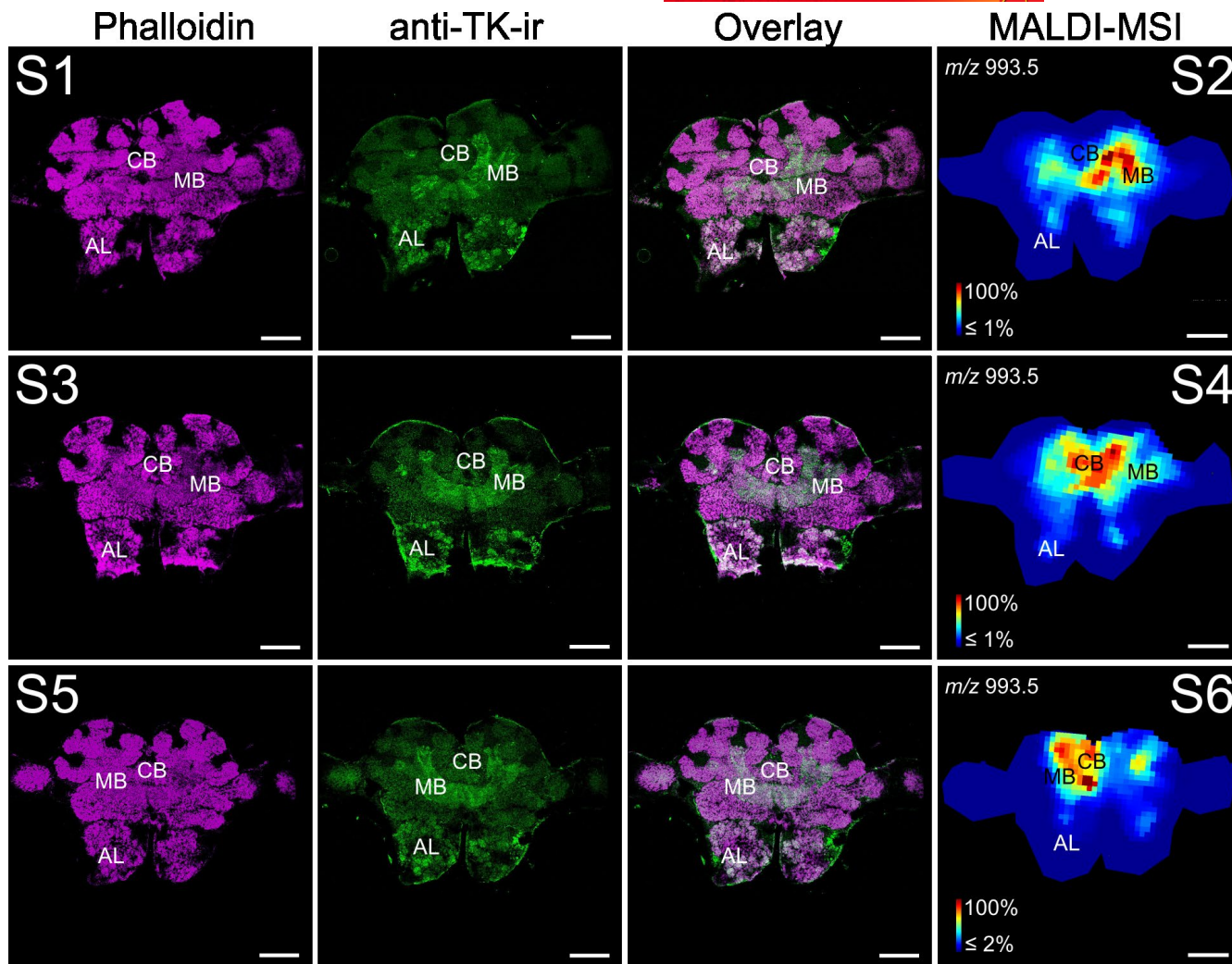
FIGURE 5 Distribution of tachykinin-related peptides (TK) analyzed in six consecutive brain sections (S1–S6) using immunohistochemistry and MALDI-MSI by the ultrafleXtreme MS instrument. The 14 μm brain sections are ordered from anterior to posterior (S1–S6). (S1, S3 and S5) Double-immunofluorescence stainings of anti-TK like-ir (green) and phalloidin labeling (magenta). F-actin labeling with phalloidin was used to identify specific neuropil regions in the brain such as the mushroom body (MB), the central body (CB) and the glomeruli of the antennal lobes (AL). Anti-TK labeling reveals the presence of anti-TK-ir in the MB, CB and the glomeruli of the AL, shifting from the right to the left hemisphere in consecutive serial sections (green). (S2, S4 and S6) Molecular images of TK-1 (*m/z* 993.5) using mass spectrometry imaging revealed the spatial distribution of TK-1 in the MB, CB as well as in the glomeruli of the AL with a similar shift from right to left in consecutive sections as shown with immunostaining. The accuracy of mass matching for peptide assignment was set to ±0.05%. Scale bars = 200 μm

neuropeptide-like, and 11 protein hormone genes (Table 1). We found that six of these precursors were translated from alternatively spliced mRNAs (*alp*, *capa*, *nplp-1*, *cch-1 cch-2*, *ilp-2*, *itp*) which potentially results in differences in the amino acid sequence of some peptides. In insects, alternatively spliced neuropeptide mRNAs are not unusual and were also found in *e.g.* the stick insect *C. morosus* (Liessem et al., 2018), locusts, termites (Veenstra, 2014), kissing bugs (Sterkel et al., 2012), and ants (Choi et al., 2014). Longer and shorter *capa* transcripts were previously described for other insects including the cockroach *P. americana* (Neupert et al., 2014), the fire ant *Solenopsis invicta* (Choi et al., 2014) and the stick insect *C. morosus* (Liessem et al., 2018). Cell-specific transcripts of CAPA peptides in individual *capa*-neurons have not been observed in cockroaches (Eckert et al., 2002; Neupert et al., 2014; Pollák

et al., 2005), but were suggested for the fire ant *S. invicta* (Choi et al., 2014) and may thus also exist for the related *C. nodus*. The novel neuropeptide-like gene *fliktin* with protein sequence similarities to uncharacterized protein precursors from other ants contains five non-amidated peptides. BLAST searches revealed highly sequence similarities of the *fliktin* gene with a *V. emeryi* protein precursor predicted as stress-response protein NST-1 by automated computational analysis and annotation from the *V. emeryi* genome and a potential neuropeptide gene designated as PaOGS36577 from the cockroach *P. americana* (Zeng et al., 2021). Furthermore, using the same annotation method as described for *V. emeryi*, an NST-1 precursor (Acc.-No. XP_033313739) was predicted from the bumblebee *Bombus bifarius*. For these insects, functional studies of the NST-1 or PaOGS36577 gene are lacking.

Transcripts for 13 insect neuropeptide genes described from other insects (*acp*, *mip*, *ast-c*, *calcitonin-a*, *-b*, *efla*, *hansolin*, *natalisin/waara*, *rya*, *proctolin*, *insect kinin*, *rfla*, and *tryptopyrokinin*) could not be found in the assembled brain transcriptome data of *C. nodus*. Genes for these neuropeptide precursors were also not found in other ant species (Nygaard et al., 2011; Schmitt et al., 2015). Our data thus supports a general absence of these peptides in ants (Formicidae), although they occur in at least some non-formicid hymenopteran species - with exception of MIP and calcitonin (Chang et al., 2018; Hummon et al., 2006) which seem to be generally missing in hymenopteran genomes.

4.2 | MS characterization of putative mature neuropeptides, neuropeptide-like, and protein hormones

To characterize the potential bioactive peptides processed from the 49 predicted precursor proteins from the brain transcriptome, we applied brain extract analysis by Q-Exactive Orbitrap MS and direct tissue profiling by MALDI-TOF MS. For most of the prepropeptide genes, we identified all predicted and likely bioactive neuropeptides by comparing calculated peptide fragments with the resulting fragmentation pattern generated by MS^2 of the ion of interest. This also includes five products from the novel *flik* gene, three of which were detected in the RCC by direct tissue profiling which indicates likely a potential hormonal function in *C. nodus*. For a few prepropeptides, predicted mature neuropeptides were confirmed by mass match only. The protein hormones ILP-1 and PTTH were not confirmed by mass spectrometry but identification of adjoining PPs indicated at least the processing of the respective prepropeptide. Furthermore, we did not detect ETH peptides in our brain samples. This is not surprising as ETH in insects is expressed exclusively in epi/peritracheal cells (Inka cells) attached to the surface of the major tracheal trunk (O'Brien & Taghert, 1998; Zitnan et al., 2003). The protein hormones NPF-1, NP, EH, bursicon alpha, and beta also did not yield positive hits. Their predicted ion mass is either above 10,000 Da and thus outside of the detection range of *m/z* 600–10,000 Da in our experiments, or their production is restricted to specific developmental time windows (e.g. EH).

4.3 | Molecular imaging of mature neuropeptides in *C. nodus* brain sections as a tool to correlate behavioral transitions with compartment-specific changes in the neuropeptidome

As outlined in the introduction, neuropeptides are prime candidates to regulate age-specific behavioral transitions in social insects. Still very little is known about which peptide signaling pathways are involved. One way to approach this interesting question is to correlate expression of given peptides with a certain age or behavior. Measuring neuropeptide content in insect brains by immunological methods (e.g. ELISA) has since long been established, and is now increasingly

performed by (semi)quantiative mass spectrometry of tissue extracts (e.g. Brockmann et al., 2009; Kunz et al., 2018; Sterkel et al., 2011) or by direct tissue profiling (*e.g.*, Wegener et al., 2011, Nagata et al., 2012, Christ et al., 2017). Yet, there is growing evidence that insect neurons of a given peptide identity do not necessarily form functionally homogenous groups and may have different functions and may act in different circuits. This seems not surprising given the comparatively low number of neurons by which insect brains fulfill astonishingly complex tasks. For example, sNPF neurons have diverse subset-specific functions in e.g. metabolic stress response (Kahsai, Kapan et al., 2010) or promotion of sleep (Shang et al., 2013). Moreover, neuropeptides are sometimes stored in excess and up-regulation and release may lead to substantial changes only at certain storage or release sites in a compartment-specific manner, especially in widely branched peptidergic neurons such as the SIFamide neurons (Dreyer et al., 2019). While not explicitly demonstrated for insect neuropeptides so far, this situation has been recently demonstrated for the other large class of neuromodulators, the biogenic amines during arousal in the honey bee brain (Ramesh & Brockmann, 2019). Thus, measuring total peptide levels over larger brain areas may mask actual changes in peptide levels that occur in either specific neurons or specific brain compartments where the peptides are released.

In our study, we used MALDI-MSI to detect the spatial distribution of mature bioactive neuropeptides and neuropeptide-like molecules within the ant brain at high spatial resolution. Different to immunolabeling, MSI enables untargeted investigation of neuropeptides in thin brain sections, and has already been used successfully to characterize age- and state-dependent changes in specific peptides in the honey bee brain (Pratavieira et al., 2014, 2018). We here optimized and standardized an MSI protocol for neuropeptide detection in ant brain sections that allows to perform similar analyses over a much broader range of peptides at high spatial resolution. For ant brains, we found that an adequate dehydration procedure of the samples in a desiccator is a crucial step to achieve sufficient neuropeptide detection. The quick removal of ethanol during the washing steps clearly improved the homogeneity of matrix crystal formation, and, thus, the reproducibility of molecular images.

The reproducibility and spatial accuracy of MALDI-MSI in small tissues has been demonstrated by comparing peptide distribution patterns obtained by immunostainings and MALDI-MSI in the neuroendocrine RCC of cockroaches (Ly et al., 2019). We now confirmed these findings for ant brain tissue and show that MSI and TK-immunostaining revealed very similar distribution patterns of TKs with pronounced labeling in the MBs, the CB and the ALs across consecutive brain tissue sections, consistent with the immunostaining pattern in the closely related ant *Cataglyphis fortis* (Schmitt et al., 2017). In general, the generated ion maps for the different neuropeptides exhibited very distinct patterns in line with our results from direct tissue profiling. For instance, in both direct tissue profiling and MALDI-MSI, CAPA/PVK and DH-31 were found in the ALs but did not occur in the MBs of the *Cataglyphis* brain. In contrast, inotocin and extended FMRFamides were exclusively found in the central brain but not in the ALs. We revealed a

pertinent pattern across various brain sections for Crz: the detection was restricted to lateral parts of the anterior brain sections (PL) and, with lower signal intensities, to parts of the medial protocerebrum. This indicates the presence of corazoninergic neurons in the PL with axonal projections to the medial protocerebrum and to the RCC where we found strong ion intensities for corazonin using direct tissue profiling. Thus, MALDI-MSI describes a morphology of corazoninergic neurons fully consistent with the highly conserved distribution in other insects including Hymenoptera such as *Apis mellifera* (Verleyen et al., 2006) and *Camponotus* ants (Schmitt et al., 2015). Importantly, the spatial reliability of our MALDI-MSI data is supported by unsupervised statistical analysis that maps out divisions in the *C. nodus* brain based on regional neuropeptide content. These divisions are fully consistent with specific neuropil regions of the *Cataglyphis* brain recently described by three-dimensional neuroanatomical reconstructions (Habenstein et al., 2020). We also used MALDI-MSI to uncover for the first time the location of products of the novel neuropeptide-like gene *flik* in an insect. This knowledge about the distribution of potential neuropeptides in the brain is an important fundamental prerequisite for future functional studies.

5 | CONCLUSION

In this study, we present a peptidomic data set for the ant *C. nodus* based on transcriptome analysis combined with three different MS approaches. This is the most comprehensive peptidomic analysis for a hymenopteran species so far. We further demonstrate that our optimized MALDI-MSI pipeline is an appropriate tool to investigate the spatial distribution of multiple neuropeptides in small ant brains. Furthermore, post-processing steps and MSI data clustering using k-means allows for correct allocation of neuropeptides to the respective neuronal region. This now sets the stage to use *C. nodus* for future studies to address brain-wide peptidomic changes correlated to age or stage- and task-specific behaviors in a social insect.

All experiments were conducted in compliance with the ARRIVE guidelines.

Open Research Badges

This article has received a badge for *Open Materials* because it provided all relevant information to reproduce the study in the manuscript. More information about the Open Practices badges can be found at https://cos.io/our-services/open-science-badges/.

ORCID

Jens Habenstein https://orcid.org/0000-0003-3589-6436
Sander Liessem https://orcid.org/0000-0002-7073-2659
Christian Wegener https://orcid.org/0000-0003-4481-3567
Reinhard Predel https://orcid.org/0000-0002-0202-6672
Wolfgang Rössler https://orcid.org/0000-0002-5195-8214
Susanne Neupert https://orcid.org/0000-0003-1562-5743

REFERENCES

Amdam, G. V., & Omholt, S. W. (2003). The hive bee to forager transition in honeybee colonies: The double repressor hypothesis. *Journal of Theoretical Biology*, *223*, 451–464. https://doi.org/10.1016/S0022-5193(03)00121-8

Beshers, S. N., & Fewell, J. H. (2001). Models of division of labor in social insects. *Annual Review of Entomology*, *46*, 413–440.

Bloch, G., Sullivan, J., & Robinson, G. (2002). Juvenile hormone and circadian locomotor activity in the honey bee *Apis mellifera*. *Journal of Insect Physiology*, *48*, 1123–1131. https://doi.org/10.1016/S0022-1910(02)00205-6

Bolger, A. M., Lohse, M., & Usadel, B. (2014). Trimmomatic: A flexible trimmer for Illumina sequence data. *Bioinformatics*, *30*, 2114–2120. https://doi.org/10.1093/bioinformatics/btu170

Brockmann, A., Annangudi, S. P., Richmond, T. A., Ament, S. A., Xie, F., Southey, B. R., Rodriguez-Zas, S. R., Robinson, G. E., & Sweedler, J. V. (2009). Quantitative peptidomics reveal brain peptide signatures of behavior. *Proceedings of the National Academy of Sciences of the United States of America*, *106*, 2383–2388. https://doi.org/10.1073/pnas.0813021106

Buchberger, A. R., DeLaney, K., Johnson, J., & Li, L. (2018). Mass spectrometry imaging: A review of emerging advancements and future insights. *Analytical Chemistry*, *90*, 240–265.

Camacho, C., Coulouris, G., Avagyan, V., Ma, N., Papadopoulos, J., Bealer, K., & Madden, T. L. (2009). BLAST+: Architecture and applications. *BMC Bioinformatics*, *10*, 421.–https://doi.org/10.1186/1471-2105-10-421

Chang, J., Zhao, J., & Tian, X. (2018). In silico prediction of neuropeptides in Hymenoptera parasitoid wasps. *PLoS One*, *13*, e0193561.–https://doi.org/10.1371/journal.pone.0193561

Chang, Z., Li, G., Liu, J., Zhang, Y., Ashby, C., Liu, D., Cramer, C. L., & Huang, X. (2015). Bridger: A new framework for de novo transcriptome assembly using RNA-seq data. *Genome Biology*, *16*, 30., https://doi.org/10.1186/s13059-015-0596-2

Chen, J., Reiher, W., Hermann-Luibl, C., Sellami, A., Cognigni, P., Kondo, S., Helfrich-Forster, C., Veenstra, J. A., & Wegener, C. (2016).

Allatostatin a signalling in *Drosophila* regulates feeding and sleep and is modulated by PDF. *PLoS Genetics*, 12, e1006346.

Chen, R., Hui, L., Sturm, R. M., & Li, L. (2009). Three dimensional mapping of neuropeptides and lipids in crustacean brain by mass spectral imaging. *Journal of the American Society for Mass Spectrometry*, 20, 1068–1077. https://doi.org/10.1016/j.jasms.2009.01.017

Chen, R., & Li, L. (2010). Mass spectral imaging and profiling of neuropeptides at the organ and cellular domains. *Analytical and Bioanalytical Chemistry*, 397, 3185–3193.

Choi, M. Y., Köhler, R., Vander Meer, R. K., Neupert, S., & Predel, R. (2014). Identification and expression of capa gene in the fire ant, Solenopsis Invicta. *PLoS One*, 9, e94274. https://doi.org/10.1371/journal.pone.0094274

Christ, P., Reifenrath, A., Kahnt, J., Hauser, F., Hill, S. R., Schachtner, J., & Ignell, R. (2017). Feeding-induced changes in allatostatin-A and short neuropeptide F in the antennal lobes affect odor-mediated host seeking in the yellow fever mosquito, Aedes aegypti. *PLoS One*, 12, e0188243.–https://doi.org/10.1371/journal.pone.0188243

Dancker, P., Low, I., Hasselbach, W., & Wieland, T. (1975). Interaction of actin with phalloidin: Polymerization and stabilization of F-actin. *Biochimica Et Biophysica Acta (BBA) - Protein Structure*, 400, 407–414. https://doi.org/10.1016/0005-2795(75)90196-8

Ddolezal, A. G., Brent, C. S., Hölldobler, B., & Amdam, G. V. (2012). Worker division of labor and endocrine physiology are associated in the harvester ant, *Pogonomyrmex californicus. Journal of Experimental Biology*, 215, 454–460.

Derst, C., Dircksen, H., Meusemann, K., Zhou, X., Liu, S., & Predel, R. (2016). Evolution of neuropeptides in non-pterygote hexapods. *BMC Evolutionary Biology*, 16, 51.

Dreyer, A. P., Martin, M. M., Fulgham, C. V., Jabr, D. A., Bai, L., Beshel, J., & Cavanaugh, D. J. (2019). A circadian output center controlling feeding: Fasting rhythms in *Drosophila. PLOS Genetics*, 15, e1008478.

Eckert, M., Herbert, Z., Pollák, E., Molnár, L., & Predel, R. (2002). Identical cellular distribution of all abundant neuropeptides in the major abdominal neurohemal system of an insect (*Periplaneta americana*). *The Journal of Comparative Neurology*, 452, 264–275.

Fleischmann, P. N., Grob, R., Müller, V. L., Wehner, R., & Rössler, W. (2018). The geomagnetic field is a compass cue in *Cataglyphis* ant navigation. *Current Biology*, 28, 1440–1444.

Fleischmann, P. N., Grob, R., Wehner, R., & Rössler, W. (2017). Species-specific differences in the fine structure of learning walk elements in *Cataglyphis* ants. *Journal of Experimental Biology*, 220, 2426–2435.

Fricker, L. D. (2012). *Neuropeptides and other bioactive peptides*. Morgan & Claypool Life Sciences.

Gasteiger, E., Gattiker, A., Hoogland, C., Ivanyi, I., Appel, R. D., & Bairoch, A. (2003). ExPASy: The proteomics server for in-depth protein knowledge and analysis. *Nucleic Acids Research*, 31, 3784–3788. https://doi.org/10.1093/nar/gkg563

Gordon, D. M. (1989). Dynamics of task switching in harvester ants. *Animal Behaviour*, 38, 194–204. https://doi.org/10.1016/S0003-3472(89)80082-X

Gospocic, J., Shields, E. J., Glastad, K. M., Lin, Y., Penick, C. A., Yan, H., Mikheyev, A. S., Linksvayer, T. A., Garcia, B. A., Berger, S. L., Liebig, J., Reinberg, D., & Bonasio, R. (2017). The neuropeptide corazonin controls social behavior and caste identity in ants. *Cell*, 170(748–759), e12. https://doi.org/10.1016/j.cell.2017.07.014

Grabherr, M. G., Haas, B. J., Yassour, M., Levin, J. Z., Thompson, D. A., Amit, I., Adiconis, X., Fan, L., Raychowdhury, R., Zeng, Q., Chen, Z., Mauceli, E., Hacohen, N., Gnirke, A., Rhind, N., di Palma, F., Birren, B. W., Nusbaum, C., Lindblad-Toh, K., ... Regev, A. (2011). Full-length transcriptome assembly from RNA-Seq data without a reference genome. *Nature Biotechnology*, 29, 644–652.

Haas, B. J., Papanicolaou, A., Yassour, M., Grabherr, M., Blood, P. D., Bowden, J., Couger, M. B., Eccles, D., Li, B., Lieber, M., Macmanes, M. D., Ott, M., Orvis, J., Pochet, N., Strozzi, F., Weeks, N., Westerman, R., William, T., Dewey, C. N., ... Regev, A. (2013). *De novo* transcript sequence reconstruction from RNA-seq using the Trinity platform for reference generation and analysis. *Nature Protocols*, 8, 1494–1512. https://doi.org/10.1038/nprot.2013.084

Habenstein, J., Amini, E., Grübel, K., el Jundi, B., & Rössler, W. (2020). The brain of *Cataglyphis* ants: Neuronal organization and visual projections. *The Journal of Comparative Neurology*, 528, 3479–3506. https://doi.org/10.1002/cne.24934

Hamilton, A., Shpigler, H., Bloch, G., Wheeler, D. E., & Robinson, G. E. (2016). *Endocrine influences on insect societies. Non-mammalian hormone-behavior systems*. Elsevier.

Han, B., Fang, Y., Feng, M., Hu, H., Qi, Y., Huo, X., Meng, L., Wu, B., & Li, J. (2015). Quantitative neuropeptidome analysis reveals neuropeptides are correlated with social behavior regulation of the honeybee workers. *Journal of Proteome Research*, 14, 4382–4393. https://doi.org/10.1021/acs.jproteome.5b00632

Hölldobler, B., & Wilson, E. O. (1990). *The ants*. Harvard University Press.

Huang, Z. Y., & Robinson, G. (1995). Seasonal changes in juvenile hormone titers and rates of biosynthesis in honey bees. *Journal of Comparative Physiology B*, 165, 18–28.

Hummon, A. B., Richmond, T. A., Verleyen, P., Baggerman, G., Huybrechts, J., Ewing, M. A., Vierstraete, E., Rodriguez-Zas, S. L., Schoofs, L., Robinson, G. E., & Sweedler, J. V. (2006). From the genome to the proteome: Uncovering peptides in the *Apis* brain. *Science*, 314, 647–649. https://doi.org/10.1126/science.1124128

Kahsai, L., Kapan, N., Dircksen, H., Winther, A. M. E., & Nässel, D. R. (2010). Metabolic stress responses in Drosophila are modulated by brain neurosecretory cells that produce multiple neuropeptides. *PLoS One*, 5, e11480. https://doi.org/10.1371/journal.pone.0011480

Kahsai, L., Martin, J. R., & Winther, A. M. (2010). Neuropeptides in the drosophila central complex in modulation of locomotor behavior. *Journal of Experimental Biology*, 213, 2256–2265.

Kamhi, J. F., & Traniello, J. F. (2013). Biogenic amines and collective organization in a superorganism: Neuromodulation of social behavior in ants. *Brain, Behavior and Evolution*, 82, 220–236. https://doi.org/10.1159/000356091

Kastin, A. J. (Ed.) (2013). *Handbook of Biologically active peptides*, 2nd edn. Academic Press.

Khatib-Shahidi, S., Andersson, M., Herman, J. L., Gillespie, T. A., & Caprioli, R. M. (2006). Direct molecular analysis of whole-body animal tissue sections by imaging MALDI mass spectrometry. *Analytical Chemistry*, 78, 6448–6456.

Knapek, S., Kahsai, L., Winther, A. M., Tanimoto, H., & Nässel, D. R. (2013). short neuropeptide F acts as a functional neuromodulator for olfactory memory in kenyon cells of *Drosophila* mushroom bodies. *Journal of Neuroscience*, 33, 5340–5345. https://doi.org/10.1523/JNEUROSCI.2287-12.2013

Ko, K. I., Root, C. M., Lindsay, S. A., Zaninovich, O. A., Shepherd, A. K., Wasserman, S. A., Kim, S. M., & Wang, J. A. (2015). Starvation promotes concerted modulation of appetitive olfactory behavior via parallel neuromodulatory circuits. *eLife*, 4, e08298.

Kohlmeier, P., Feldmeyer, B., & Foitzik, S. (2018). Vitellogenin-like a–associated shifts in social cue responsiveness regulate behavioral task specialization in an ant. *PLOS Biology.*, 16, e2005747. https://doi.org/10.1371/journal.pbio.2005747

Kunz, T. O., Chen, J., & Wegener, C. (2018). Metabolic labeling to quantify drosophila neuropeptides and peptide hormones. *Methods in Molecular Biology*, 1719, 175–185.

Liessem, S., Ragionieri, L., Neupert, S., Büschges, A., & Predel, R. (2018). Transcriptomic and neuropeptidomic analysis of the stick insect, *Carausius morosus. Journal of Proteome Research*, 17, 2192–2204.

Ly, A., Ragionieri, L., Liessem, S., Becker, M., Deininger, S. O., Neupert, S., & Predel, R. (2019). Enhanced coverage of insect neuropeptides in tissue sections by an optimized mass-spectrometry-imaging protocol. *Analytical Chemistry*, 91, 1980–1988.

Nagata, S., Matsumoto, S., Nakane, T., Ohara, A., Morooka, N., Konuma, T., Nagai, C., & Nagasawa, H. (2012). Effects of starvation on brain short neuropeptide F-1, -2, and -3 levels and short neuropeptide F receptor expression levels of the Silkworm, Bombyx Mori. *Frontiers in Endocrinology*, *3*, 3. https://doi.org/10.3389/fendo.2012.00003

Nässel, D. R., & Zandawala, M. (2019). Recent advances in neuropeptide signaling in drosophila, from genes to physiology and behavior. *Progress in Neurobiology*, *179*, 101607.

Neupert, S., Derst, C., Sturm, S., & Predel, R. (2014). Identification of two Capa cDNA transcripts and detailed peptidomic characterization of their peptide products in *Periplaneta americana*. *EuPa Open Proteomics*, *3*, 195–205. https://doi.org/10.1016/j.euprot.2014.02.005

Nygaard S., Zhang G., Schiøtt M., Li C., Wurm Y., Hu H., Zhou J., Ji L., Qiu F., Rasmussen M., Pan H., Hauser F., Krogh A., Grimmelikhuijzen C. J., Wang J., & Boomsma J. J. (2011) The genome of the leaf-cutting ant Acromyrmex echinatior suggests key adaptations to advanced social life and fungus farming. *Genome Research*. *21*, 1339–1348. https://doi.org/10.1101/gr.121392.111

O'Brien, M. A., & Taghert, P. H. (1998). A peritracheal neuropeptide system in insects: Release of myomodulin-like peptides at ecdysis. *Journal of Experimental Biology*, *201*, 193–209.

Oster, G. F., & Wilson, E. O. (1978). *Caste and ecology in the social insects*. Princeton University Press.

Pauls, D., Chen, J., Reiher, W., Vanselow, J. T., Schlosser, A., Kahnt, J., & Wegener, C. (2014). Peptidomics and processing of regulatory peptides in the fruit fly *Drosophila*. *EuPA Open Proteomics*, *3*, 114–127. https://doi.org/10.1016/j.euprot.2014.02.007

Pollák, E., Eckert, M., Molnár, L., & Predel, R. (2005). Differential sorting and packaging of *capa*-gene related products in an insect. *The Journal of Comparative Neurology*, *481*, 84–95.

Pratavieira, M., da Silva Menegasso, A. R., Garcia, A. M., dos Santos, D. S., Gomes, P. C., Malaspina, O., & Palma, M. S. (2014). MALDI imaging analysis of neuropeptides in the africanized honeybee (*Apis mellifera*) brain: Effect of ontogeny. *Journal of Proteome Research*, *13*, 3054–3064.

Pratavieira, M., Menegasso, A. R. D. S., Esteves, F. G., Sato, K. U., Malaspina, O., & Palma, M. S. (2018). MALDI Imaging analysis of neuropeptides in Africanized Honeybee (*Apis mellifera*) brain: Effect of aggressiveness. *Journal of Proteome Research*, *17*, 2358–2369.

Predel, R., Neupert, S., Derst, C., Reinhardt, K., & Wegener, C. (2018). Neuropeptidomics of the bed bug *Cimex lectula*rius. *Journal of Proteome Research*, *17*, 440–454.

Predel, R., Neupert, S., Garczynski, S. F., Crim, J. W., Brown, M. R., Russell, W. K., Kahnt, J., Russell, D. H., & Nachman, R. J. (2010). Neuropeptidomics of the mosquito *Aedes aegypti*. *Journal of Proteome Research*, *9*, 2006–2015.

Ramesh, D., & Brockmann, A. (2019). Mass spectrometric quantification of arousal associated neurochemical changes in single honey bee brains and brain regions. *ACS Chemical Neuroscience*, *10*, 1950–1959.

Rappsilber, J., Mann, M., & Ishihama, Y. (2007). Protocol for micropurification, enrichment, pre-fractionation and storage of peptides for proteomics using StageTips. *Nature Protocols*, *2*, 1896–1906.

Robinson, G. E. (1987). Regulation of honey bee age polyethism by juvenile hormone. *Behavioral Ecology and Sociobiology*, *20*, 329–338. https://doi.org/10.1007/BF00300679

Robinson, G. E. (1992). Regulation of division of labor in insect societies. *Annual Review of Entomology*, *37*, 637–665. https://doi.org/10.1146/annurev.en.37.010192.003225

Ronacher, B. (2008). Path integration as the basic navigation mechanism of the desert ant *Cataglyphis fortis* (Forel, 1902) (Hymenoptera: Formicidae). *Myrmecological News*, *11*, 53–62.

Rössler, W. (2019). Neuroplasticity in desert ants (Hymenoptera: Formicidae) – importance for the ontogeny of navigation. *Myrmecological News*, *29*, 1–20.

Schachtner, J., Wegener, C., Neupert, S., & Predel, R. (2010). Direct peptide profiling of brain tissue by MALDI-TOF mass spectrometry. *Methods in Molecular Biology*, *615*, 129–135.

Schindelin, J., Arganda-Carreras, I., Frise, E., Kaynig, V., Longair, M., Pietzsch, T., Preibisch, S., Rueden, C., Saalfeld, S., Schmid, B., Tinevez, J. Y., White, D. J., Hartenstein, V., Eliceiri, K., Tomancak, P., & Cardona, A. (2012). Fiji: An open-source platform for biological-image analysis. *Nature Methods*, *9*, 676–682. https://doi.org/10.1038/nmeth.2019

Schmitt, F., Vanselow, J. T., Schlosser, A., Kahnt, J., Rössler, W., & Wegener, C. (2015). Neuropeptidomics of the carpenter ant *Camponotus floridanus*. *Journal of Proteome Research*, *14*, 1504–1514.

Schmitt, F., Vanselow, J. T., Schlosser, A., Wegener, C., & Rössler, W. (2017). Neuropeptides in the desert ant *Cataglyphis fortis*: Mass spectrometric analysis, localization, and age-related changes. *The Journal of Comparative Neurology*, *525*, 901–918.

Scholl, C., Wang, Y., Krischke, M., Mueller, M. J., Amdam, G. V., & Rössler, W. (2014). Light exposure leads to reorganization of microglomeruli in the mushroom bodies and influences juvenile hormone levels in the honeybee. *Developmental Neurobiology*, *74*, 1141–1153. https://doi.org/10.1002/dneu.22195

Schoofs, L., de Loof, A., & van Hiel, M. B. (2017). Neuropeptides as regulators of behavior in insects. *Annual Review of Entomology*, *62*, 35–52. https://doi.org/10.1146/annurev-ento-031616-035500

Seid, M. A., & Traniello, J. F. (2005). Age-related changes in biogenic amines in individual brains of the ant *Pheidole dentata*. *Naturwissenschaften*, *92*, 198–201. https://doi.org/10.1007/s00114-005-0610-8

Shang, Y., Donelson, N. C., Vecsey, C. G., Guo, F., Rosbash, M., & Griffith, L. C. (2013). Short neuropeptide F is a sleep-promoting inhibitory modulator. *Neuron*, *80*, 171–183. https://doi.org/10.1016/j.neuron.2013.07.029

Smith-Unna, R., Boursnell, C., Patro, R., Hibberd, J. M., & Kelly, S. (2016). TransRate: Reference-free quality assessment of de novo transcriptome assemblies. *Genome Research*, *26*, 1134–1144. https://doi.org/10.1101/gr.196469.115

Sterkel, M., Oliveira, P. L., Urlaub, H., Hernandez-Martinez, S., Rivera-Pomar, R., & Ons, S. (2012). OKB, a novel family of brain-gut neuropeptides from insects. *Insect Biochemistry and Molecular Biology*, *42*, 466–473. https://doi.org/10.1016/j.ibmb.2012.03.003

Sterkel, M., Urlaub, H., Rivera-Pomar, R., & Ons, S. (2011). Functional proteomics of neuropeptidome dynamics during the feeding process of *Rhodnius prolixus*. *Journal of Proteome Research*, *10*, 3363–3371.

Sullivan, J. P., Jassim, O., Fahrbach, S. E., & Robinson, G. E. (2000). Juvenile hormone paces behavioral development in the adult worker honey bee. *Hormones and Behavior.*, *37*, 1–14. https://doi.org/10.1006/hbeh.1999.1552

Takeuchi, H., Yasuda, A., Yasuda-Kamatani, Y., Kubo, T., & Nakajima, T. (2003). Identification of a tachykinin-related neuropeptide from the honeybee brain using direct MALDI-TOF MS and its gene expression in worker, queen and drone heads. *Insect Molecular Biology*, *12*, 291–298. https://doi.org/10.1046/j.1365-2583.2003.00414.x

Trede, D., Schiffler, S., Becker, M., Wirtz, S., Steinhorst, K., Strehlow, J., Aichler, M., Kobarg, J. H., Oetjen, J., Dyatlov, A., Heldmann, S., Walch, A., Thiele, H., Maass, P., & Alexandrov, T. (2012). Exploring three-dimensional matrix-assisted laser desorption/ionization imaging mass spectrometry data: Three-dimensional spatial segmentation of mouse kidney. *Analytical Chemistry*, *84*, 6079–6087.

Urlacher, E., Soustelle, L., Parmentier, M. L., Verlinden, H., Gherardi, M. J., Fourmy, D., Mercer, A. R., Devaud, J. M., & Massou, I. (2016). Honey bee allatostatins target galanin/somatostatin-like receptors and modulate learning: A conserved function? *PLoS One*, *11*, e0146248.–https://doi.org/10.1371/journal.pone.0146248

Veenstra, J. A. (2000). Mono- and dibasic proteolytic cleavage sites in insect neuroendocrine peptide precursors. *Archives of Insect Biochemistry and Physiology*, *43*, 49–63.

Veenstra, J. A. (2014). The contribution of the genomes of a termite and a locust to our understanding of insect neuropeptides and neurohormones. *Frontiers in Physiology*, *5*, 454.

Verhaert, P. D., Prieto Conaway, M. C., Pekar, T. M., & Miller, K. (2007). Neuropeptide imaging on an LTQ with vMALDI source: The complete 'all-in-one' peptidome analysis. *International Journal of Mass Spectrometry*, *260*, 177–184. https://doi.org/10.1016/j.ijms.2006.11.008

Verleyen, P., Baggerman, G., Mertens, I., Vandersmissen, T., Huybrechts, J., Van Lommel, A., De Loof, A., & Schoofs, L. (2006). Cloning and characterization of a third isoform of corazonin in the honey bee *Apis mellifera*. *Peptides*, *27*, 493–499. https://doi.org/10.1016/j.peptides.2005.03.065

Wagener-Hulme, C., Kuehn, J., Schulz, D., & Robinson, G. (1999). Biogenic amines and division of labor in honey bee colonies. *Journal of Comparative Physiology A*, *184*, 471–479.

Warner, M. R., Mikheyev, A. S., & Linksvayer, T. A. (2019). Transcriptomic basis and evolution of the ant nurse-larval social interactome. *PLoS Genetics*, *15*, e1008156. https://doi.org/10.1371/journal.pgen.1008156

Wegener, C., Herbert, H., Kahnt, J., Bender, M., & Rhea, J. M. (2011). Deficiency of prohormone convertase dPC2 (AMONTILLADO) results in impaired production of bioactive neuropeptide hormones in Drosophila. *Journal of Neurochemistry*, *118*, 581–595. https://doi.org/10.1111/j.1471-4159.2010.07130.x

Wehner, R. (2009). The architecture of the desert ant's navigational toolkit (Hymenoptera: 1404 Formicidae). *Myrmecological News*, *12*, 85–96.

Winther, A. M., Acebes, A., & Ferrus, A. (2006). Tachykinin-related peptides modulate odor perception and locomotor activity in *Drosophila*. *Molecular and Cellular Neurosciences*, *31*, 399–406. https://doi.org/10.1016/j.mcn.2005.10.010

Wurm, Y., Wang, J., Riba-Grognuz, O., Corona, M., Nygaard, S., Hunt, B. G., Ingram, K. K., Falquet, L., Nipitwattanaphon, M., Gotzek, D., Dijkstra, M. B., Oettler, J., Comtesse, F., Shih, C. J., Wu, W. J., Yang, C. C., Thomas, J., Beaudoing, E., Pradervand, S., … Keller, L. (2011). The genome of the fire ant *Solenopsis invicta*. *Proceedings of the National Academy of Sciences of the United States of America*, *108*, 5679–5684.

Yang, A. (2006). Seasonality, division of labor, and dynamics of colony-level nutrient storage in the ant *Pheidole morrisi*. *Insectes Sociaux*, *53*, 456–462. https://doi.org/10.1007/s00040-005-0896-3

Yang, J., & Caprioli, R. M. (2011). Matrix sublimation/recrystallization for imaging proteins by mass spectrometry at high spatial resolution. *Analytical Chemistry*, *83*, 5728–5734.

Zeng, H., Qin, Y., Du, E., Wei, Q., Li, Y., Huang, D., Wang, G., Veenstra, J. A., Li, S., & Li, N. (2021). Genomics- and peptidomics-based discovery of conserved and novel neuropeptides in the American Cockroach. *Journal of Proteome Research*, *20*, 1217–1228. https://doi.org/10.1021/acs.jproteome.0c00596

Zitnan, D., Zitnanová, I., Spalovská, I., Takác, P., Park, Y., & Adams, M. E. (2003). Conservation of ecdysis-triggering hormone signalling in insects. *Journal of Experimental Biology*, *206*, 1275–1289.

SUPPORTING INFORMATION

Additional supporting information may be found online in the Supporting Information section.